3 Principles of Crystal Nucleation and Growth

James J. De Yoreo

Chemistry and Materials Science Directorate
Lawrence Livermore National Laboratory
Livermore, California 94551 U.S.A.

Peter G. Vekilov

Department of Chemical Engineering
University of Houston
Houston, Texas 77204 U.S.A.

INTRODUCTION

In the most general sense, biomineralization is a process by which organisms produce materials solutions for their own functional requirements. Because so many biomineral products are derived from an initial solution phase and are either completely crystalline or include crystalline components, an understanding of the physical principles of crystallization from solutions is an important tool for students of biomineralization. However, crystal growth is a science of great breadth and depth, about which many extensive texts have been written. In addition, there are already other thorough reviews that specifically address the crystal growth field of study as it relates to biomineral formation. Consequently, the goals of this chapter are both modest and specific. It is intended to provide: 1) a simple narrative explaining the physical principles behind crystallization for those who are completely new to the topic, 2) a few basic equations governing nucleation and growth for those who wish to apply those principles—at least in a semi-quantitative fashion—to experimental observations of mineralization, and 3) an overview of some recent molecular-scale studies that have revealed new insights into the control of crystal growth by small molecules, both organic and inorganic.

This last topic gets to the heart of what makes crystallization in biological systems unique. Every day, many tons of crystals are produced synthetically in non-biological processes, but by-and-large, the degree of control over nucleation and growth achieved by deterministic additions of growth modifiers or the presence of a controlling matrix is very minor. More commonly, crystal growers view modifying agents as unwanted impurities and work extremely hard to eliminate them from the starting materials. Indeed, the degree to which living organisms are able to control the crystallization process is most striking when contrasted to the products of such synthetic crystallization processes. This contrast applies to both the compositional differences that result (e.g., Weiner and Dove 2003) and the external morphology. Figure 1a shows a typical photomicrograph of a crystal of calcium carbonate grown in a closed beaker from a pure solution. It has a simple rhombohedral shape and consists of calcite, the most stable form of calcium carbonate. Moreover, crystals grown in this way tend to nucleate randomly throughout the beaker or on its surfaces with no preferred orientation and grow at a rate determined by the solution conditions as well as various inherent materials parameters. Figure 1b-d shows examples of biological calcite in the form of shaped single crystals, intricate crystal composites, and regular crystal laminates. The calcite crystals, as coccolith plates (Fig. 1b), lie in specific locations and are oriented with respect to the crystallographic axes of calcite; whereas the mollusk shell crystallites (Fig. 1c) are aragonite, which in standard laboratory conditions is a less stable form of calcium carbonate than is calcite. The calcite crystals from the human inner ear (Fig. 1d) exhibit a spindle-like shape that is

1529-6466/03/0054-0003$05.00

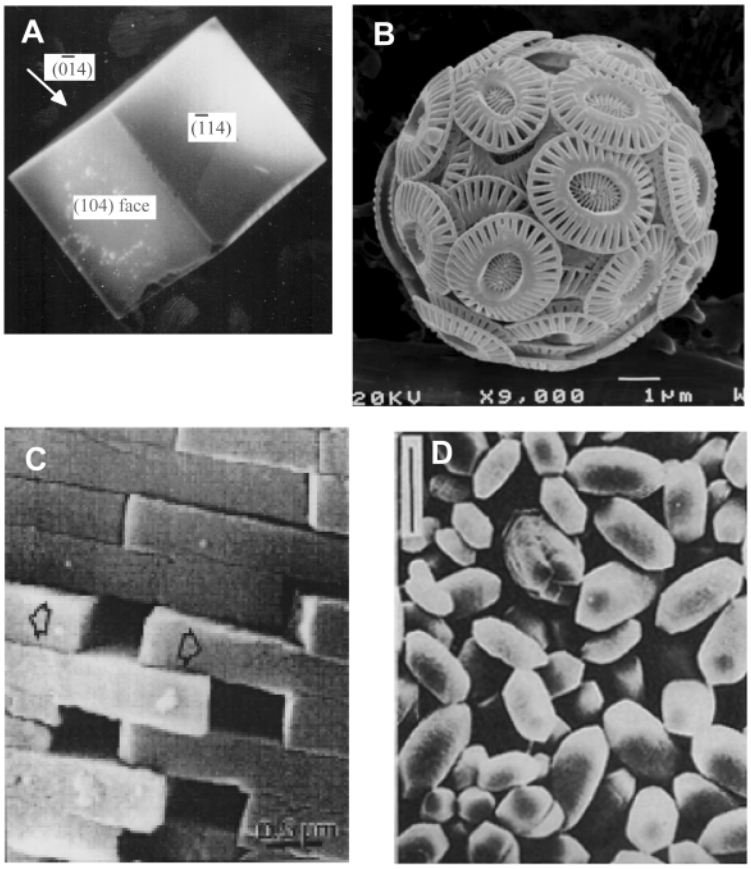

Figure 1. Scanning electron micrographs of (A) synthetic calcite, (B) Coccolithophorid, *Emiliania huxleyi* (from International Nannoplankton Association website), (C) Aragonitic layers from Mollusc shell (From Calvert 1992 with permission from Materials Research Society), and (D) calcite crystals from the human inner ear (From Mann 2001 with permission from Oxford University Press).

quite different from that of synthetic calcite. These examples demonstrate that organisms are able to control the location and crystallographic orientation of nucleation, the shape of the growing crystallites, and even the phase of the resulting material.

One of the major challenges in crystal growth science today is to understand the physical mechanisms by which this level of control is achieved. A very general and useful construct for thinking about the problem is the "energy landscape," illustrated in Figure 2. This landscape highlights the fact that crystallization is, first and foremost, a phase transition through which matter is transformed from a state of high free energy in a solvated state to one of low free energy in the crystal lattice. All aspects of a crystal, including its phase, habit, and growth rate, are determined by the shape of this landscape. Equilibrium crystal habit and phase are controlled by the depths and shapes of the energy minima. By varying the heights of the barriers, the growth kinetics can be controlled, and non-equilibrium final or intermediate states can be selected. It stands to reason that living organisms modulate crystal growth by manipulating the energy landscapes. A complete physical picture of biomineral growth requires a description of the geometry and stereochemistry of the interaction between the crystal lattice and the organic modifiers, the magnitude of the interaction energy, the effect of that interaction on the energy landscape, and the impact of the change in the landscape on crystallization.

Finally, we note that this physiochemical picture provides only a small piece to the

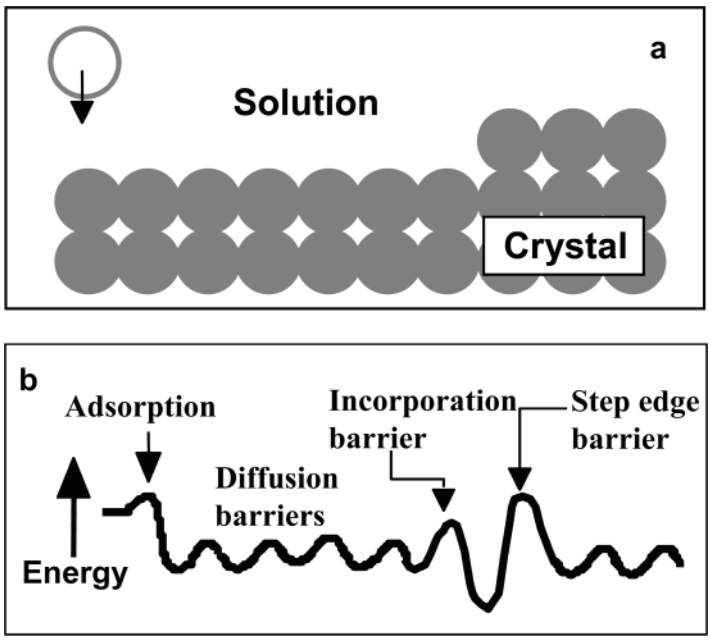

Figure 2. Schematic of (a) physical landscape and (b) energy landscape seen by a solute molecule as it becomes part of the crystal. The vertical axis in (b) can either refer to the actual potential energy if tied directly to the physical landscape, or the free energy if referring to processes encountered in the transformation to the solid state, such as dehydration or incorporation.

puzzle of biomineralization. As Figure 3 illustrates, there are many levels of regulation at work that influence these physical processes (Mann 2001). While they include other physical parameters such as spatial constraints and controls over ion fluxes, these are, in turn, influenced by a myriad of biological machines that shuttle reactants and products to desired locations, undoubtedly utilizing biochemical feedback. These processes are further influenced by a combination of genetic and environmental factors.

CRYSTAL NUCLEATION VS. CRYSTAL GROWTH

The association of organic compounds with biomineralized structures (Wada and Fujinuki 1976; Crenshaw 1972; Collins et al. 1992) and their observed effect on crystallization kinetics (Sikes et al. 1990; Wheeler et al. 1990) strongly suggest that these compounds modify the growth stage of minerals. This conclusion is reinforced by observations of faceted crystal surfaces in a number of cases, including the calcite crystals shown in Figure 1d as well as numerous examples of calcium oxalate monohydrate crystals, both functional—as in plants—and pathogenic—as in humans (Fig. 4). On the other hand, many biomineralized structures in nature suggest that organic components also control nucleation. In particular, the growth of biominerals in precise locations within complex crystal composites and the generation of crystallites with specific crystallographic orientations are difficult to explain without appealing to active controls during the nucleation stage. Moreover, there is a substantial body of evidence to suggest that proteins and other organic molecules serve as "templates," providing preferential sites for nucleation and controlling the orientation of the resulting crystals. Many organic-inorganic composites, including the shells of birds' eggs (Fink et al. 1992) and mollusks (Calvert 1992), exhibit a layered structure in which the inorganic component grows at the organic-solution interface. One of the most remarkable examples is that of bone. The carbonated apatite crystals that give bone its stiffness grow amongst

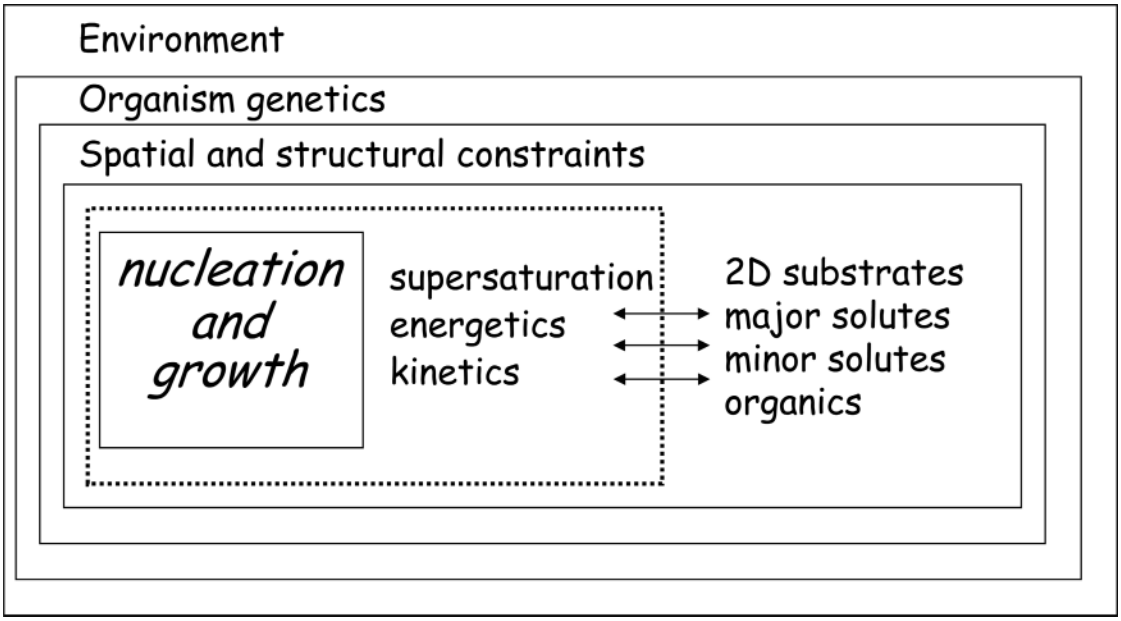

Figure 3. Levels of regulation in biomineralization. (from Dove et al. 2004, based on Mann 2001).

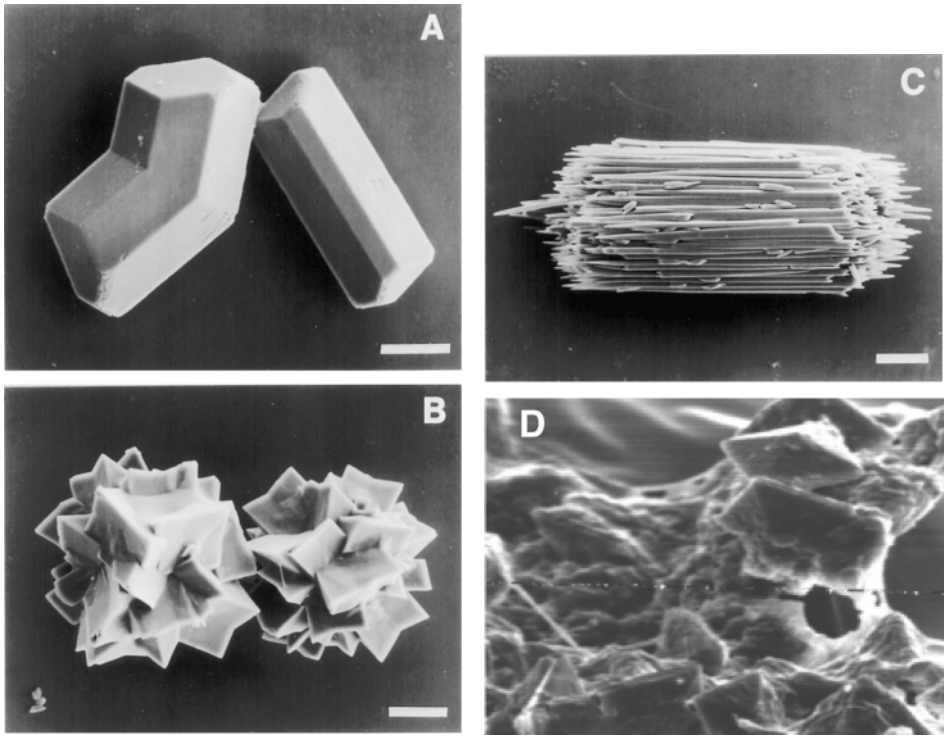

Figure 4. Scanning electron micrographs of calcium oxalate crystals. (A-C) Crystals isolated from selected plants. Scale bar = 5 μm. (A) Twinned, prismatic crystals from the seed coat of bean (*Phaseolus vulgaris*). (B) Druse crystals isolated from velvet leaf (*Abutilon theophrasti*), a common weed. (C) Isolated bundle of raphides, needle-shaped crystals, from leaves of grape (*Vitis labrusca*). (From Webb 1999 with permission from the American Society of Plant Biologists.) (D) Crystals grown in vivo on uretal stent. Crystals are about 50 mm in size. (Used with kind permission of Professor Heywood).

molecular fibers of collagen. But the location and orientation of the crystallites is not random. The collagen fibers are believed to pack into bundles with a periodicity that leaves rows of small gaps known as "hole zones" 40 nm in length and 5 nm in width, each of which provides an identical molecular-scale environment for mineralization, as illustrated in Figure 5 (Katz and Li 1973; Miller 1984; Mann 2001). The crystallites themselves grow with a specific geometric relationship between the crystal lattice and the collagen fibers, with the {001} axis lying along the length of the fiber and the {110} axis pointing along the rows of hole zones. This implies molecular-scale control by the collagen molecules over both the orientation and location of the crystal nuclei.

THERMODYNAMIC DRIVERS OF CRYSTALLIZATION

Whether considering nucleation or growth, the reason for the transformation from solution to solid is the same, namely the free energy of the initial solution phase is greater than the sum of the free energies of the crystalline phase plus the final solution phase (Gibbs 1876, 1878). In terms of solution activities (which are often well approximated by solution concentrations), an equivalent statement is that the actual activity product of the reactants, AP, exceeds the equilibrium activity product of those reactants, the latter being simply the equilibrium constant, K_{sp}. In cases where a single chemical component crystallizes, the driving force has been expressed not in terms of total free energy change during crystallization, but rather as the change in chemical potential of the crystallizing species, $\Delta\mu$. This $\Delta\mu$ measures the free energy response to molecules transferring from one phase to the other. The larger $\Delta\mu$ becomes, the greater is the driving force for crystallization (Mullin 1992).

Not surprisingly, both the change in free energy and the change in chemical potential are directly related to the activity products (Johnson 1982). For the precipitation reaction:

$$aA + bB + \ldots + nN \rightarrow A_aB_b\cdots N_n \tag{1}$$

the activity product of the reactants, AP, and the value of K_{sp} are given by:

$$AP = [A]^a[B]^b[C]^c\cdots[N]^n \tag{2}$$

$$K_{sp} = [A]_e^a[B]_e^b[C]_e^c\cdots[N]_e^n \tag{3}$$

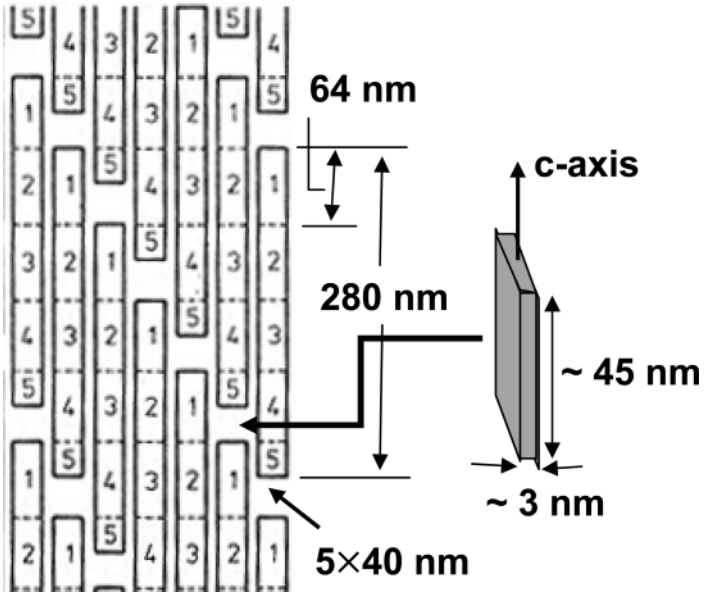

Figure 5. Schematic of collagen fibrils showing the stagger of the hole zones and the size and orientation of the carbonated hydroxyapatite crystals relative to the fibril direction. (Based on Mann 2001).

where the subscript "e" refers to the activity at equilibrium. In turn, the free energy of solution per molecule, Δg_{sol}, and the change in chemical potential are:

$$\Delta g_{sol} = -k_B T \ln K_{sp} \tag{4}$$

$$\Delta\mu = k_B T \ln AP - \Delta g_{sol} \tag{5a}$$

$$= k_B T \ln(AP/K_{sp}) \tag{5b}$$

where k_B is the Boltzmann constant, and T is the absolute temperature. Rather than use $\Delta\mu$, most crystal growth analyses refer to the supersaturation, σ, which is related to $\Delta\mu$ by:

$$\Delta\mu = k_B T \ln\sigma \tag{6}$$

$$\sigma \equiv \ln\{AP/K_{sp}\} \tag{7}$$

Readers may often see σ defined as $(AP/K_{sp}) - 1$ or even $(C/C_e) - 1$ where C and C_e are the equilibrium reactant concentrations. These are referred to as absolute supersaturations. They are valid approximations only at small values of σ and, in the case of the expression that utilizes concentrations, only useful when either the activity coefficients, $\chi = [N]/C$ and $\chi_e = [N_e]/C_e$ for the reactants are close to unity, or when $\chi = \chi_e$. Nonetheless the absolute supersaturation is important when considering the kinetics of growth. This will become clear later in the chapter.

In the sections that follow, the way in which σ and $(AP - K_{sp})$ influence nucleation and growth will be presented in detail, but it is instructive at this point to discuss, in a general sense, the external factors that can influence these parameters, since crystal growth can be modulated through their manipulation. The values of K_{sp} and C_e depend on solution composition and temperature as, to some extent, do the values of the activity coefficients, but presumably temperature variation is not an important tool for biological systems. Consequently, in order to manipulate these parameters, organisms must rely primarily on variations in solution chemistry, including ionic strength, pH, and impurity content, whether inorganic or organic.

One other important factor worth discussing is the role of water. It has recently been realized that the structuring of water molecules around ions, molecules, and colloid-sized particles in dissolved state is an important factor in the thermodynamics of phase transitions in solution. In some cases, it was found that the structured water molecules are released when the ions or molecules join a growing crystal (Yau et al. 2000a), while in other cases, additional water molecules are trapped during crystal formation (Vekilov et al. 2002a). The release or trapping of water molecules has significant enthalpic and entropic consequences. The enthalpy effect depends on the strength of the bonds between water and solute molecules and the strength of the bonds forming in the crystals. Hence, it varies significantly from system to system. The entropy effect, however, appears to be consistently ~20 J K^{-1} per mole of water released or trapped, with a positive sign in the cases of release and negative sign in the cases of trapping. Not surprisingly, the magnitude of the entropy effect above is comparable to the entropy loss upon freezing of water (Tanford 1994; Dunitz 1994).

Especially with larger species such as proteins, the entropy contribution due to solvent trapping or release can be very significant and can even be the determinant of the free energy change for crystallization. For example, it was found that the enthalpy effect of crystallization of the protein apoferritin is negligible, and crystallization occurs only because of the significant entropy gain due to the release of just one or two water molecules in each of the 12 intermolecular contacts in the crystal (Yau et al. 2000a). This entropy gain adds up to positive (+160 J K^{-1}) per mole of apoferritin, with a free energy

contribution of about –47 kJ mol^{-1}. An even more striking example is the human mutant hemoglobin C, which has a significant positive enthalpy of crystallization of 160 kJ mol^{-1}, i.e., crystallization is only possible because of the release of about 10 water molecules when a crystal contact is formed. In this case, the total entropy gain due to this release is about 600 J K^{-1} per mole of hemoglobin, and its contribution to the free energy of crystallization is –180 kJ mol^{-1}, making the net gain of free energy upon crystallization about –20 kJ mol^{-1} (Vekilov et al. 2002a).

Note that this discussion of the effects of water structuring focuses only on the contributions to the initial and final states on the free energy landscape. As discussed below in relation to the kinetics of crystallization, water structuring is also the most important contributor to the free energy barrier for crystallization, and the kinetics of restructuring of the water associated with a solute molecule seems to determine the overall crystallization rate.

NUCLEATION

Nucleation is one of the two major mechanisms of the first order phase transition, the process of generating a new phase from an old phase whose free energy has become higher than that of the emerging new phase (Hohenberg and Halperin 1977; Chaikin and Lubensky 1995). Nucleation occurs via the formation of small embryos of the new phase inside the large volume of the old phase. Another prominent feature of nucleation is metastability of the old phase, i.e., the transformation requires passage over a free energy barrier (Kashchiev 1999). This is easily understood by considering the free energy changes associated with the formation of the nucleus. The statement that the free energy per molecule of the new phase is less than that of the solvated phase only applies to the bulk of the new phase. The surface is a different matter. Because the surface molecules are less well bound to their neighbors than are those in the bulk, their contribution to the free energy of the new phase is greater. The difference between the free energy per molecule of the bulk and that of the surface is referred to as the interfacial free energy. (It is sometimes called the surface free energy, but, strictly speaking, this term should be reserved for surfaces in contact with vacuum.) The interfacial free energy is always a positive term and acts to destabilize the nucleus. As a consequence, at very small size when many of the molecules reside at the surface, the nucleus is unstable. Adding even one more molecule just increases the free energy of the system. On average, such a nucleus will dissolve rather than grow. But once the nucleus gets large enough, the drop in free energy associated with formation of the bulk phase becomes sufficiently high that the surface free energy is unimportant, and every addition of a molecule to the lattice lowers the free energy of the system. There is an intermediate size at which the free energy of the system is decreased whether the nucleus grows or dissolves, and this is known as the critical size. This phenomenon is referred to as the Gibbs-Thomson effect. Of course, if the supersaturation is high enough, the critical size can be reduced to less than one growth unit. Then the barrier vanishes and the old phase becomes unstable so that an infinitesimal fluctuation of an order parameter, such as density, can lead to the appearance of the new phase. The rate of generation and growth of the new phase is then only limited by the rate of transport of mass or energy. This second process is referred to as spinodal decomposition, and the boundary between the regions of metastability and instability of the old phase is called a spinodal line (Binder and Fratzl 2001; Kashchiev 2003).

The existence of a critical size has a number of implications. First and foremost, because nucleation of the new phase is the result of fluctuations that bring together sufficient numbers of molecules to exceed the critical size, the probability of nucleation will be strongly affected by the value of the critical size. This means that nucleation can

be controlled, to some extent, by modulating the critical size, which is in turn a function of the interfacial energy. The smaller the interfacial energy, the smaller the critical size and the more likely nucleation becomes for any given supersaturation. As a consequence, by varying either the solution composition or the supersaturation, the probability of nucleation can be manipulated.

Nucleation on foreign surfaces

The presence of a foreign surface can be used to exert even greater control over nucleation because, quite often, the interfacial energy between a crystal nucleus and a solid substrate is lower than that of the crystal in contact with the solution (Neilsen 1964; Abraham 1974; Chernov 1984; Mullin 1992; Mutaftschiev 1993). This is because the molecules in the crystal can form bonds with those in the substrate that are stronger than the bonds of solvation. Because the enthalpic contribution to the free energy comes primarily from chemical bonding, stronger bonds lead to a smaller interfacial free energy. This may well be the key physical phenomenon that allows living organisms to delineate both location and orientation of crystallites. Clearly, the strength of bonding at the interface is strongly dependent on the structure and chemistry of the substrate surface. If the atomic structure of the substrate surface closely matches a particular plane of the nucleating phase so that lattice strain is minimized and, in addition, the substrate presents a set of chemical functionalities that promote strong bonding to the nucleus, then the enthalpic contribution to the interfacial free energy becomes small, and nucleation occurs preferentially on that crystal plane.

As discussed in the introduction, many lines of evidence suggest that organisms utilize this principle to control the location and orientation of nuclei. In addition, several experimental studies (Mann et al 1992; Heywood and Mann 1994; Wong et al. 1994; Berman et al. 1995; Archibald et al. 1996; Addadi et al. 1998; Aizenberg et al. 1999a,b, 2003; Travaille et al. 2002) have used successfully used organic films to mimic the process. For example, Addadi et al. (1997) showed that β-sheet polyaspartate adsorbed onto sulfonated polystyrene substrates induced nucleation of (001) oriented calcite crystals. Acidic glycoproteins from mollusk shells had similar effects *in vitro*. Aizenberg et al. (1999a,b) showed that varying the structure of terminal groups on self-assembled monolayers (SAMs) of alkane thiols on gold precisely controlled the plane of nucleation of calcite and Travaille et al. (2002) demonstrated a 1:1 relationship between the underlying gold structure and the in-plane calcite orientation. Based on the above discussion, it is difficult to interpret these observations in any way other than the result of varying the interfacial energy. Nonetheless, little or no work has been done to quantify the relative importance of thermodynamic control through variations in interfacial energy, local increases in supersaturation due to changes in pH or ion concentration near the surface films, or even kinetic controls on adsorption/desorption rates that affect surface adsorption lifetimes and thus rates of nucleation.

We can quantify these concepts by considering the dependence of the change in free energy during precipitation on the size of the nucleus (Kashchiev 1999; Mullin 1992). For simplicity, we consider a spherical nucleus of radius r, as illustrated in Figure 6a, nucleating within the bulk solution. (This is referred to as homogeneous nucleation.) The free energy change per molecule (Δg) is given by the sum of bulk (Δg_b) and surface terms (Δg_s), namely:

$$\Delta g = \Delta g_b + \Delta g_s \tag{8a}$$

$$= - \{[(4/3)\pi r^3]/\Omega\}\Delta\mu + 4\pi r^2\alpha \tag{8b}$$

where Ω is the volume per molecule, and α is the interfacial free energy. The first term is

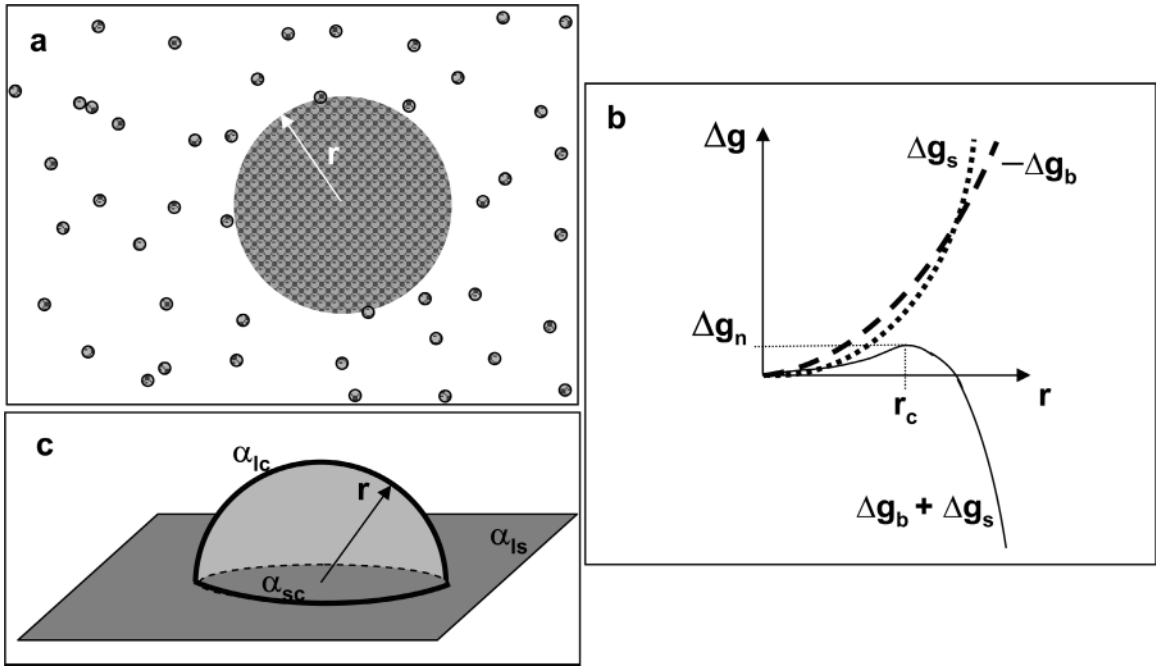

Figure 6. (a) Formation of a spherical nucleus of radius r from a solution leads to the free energy changes shown in (b). The cross-over of the bulk and surface terms combined with their opposing signs leads to a free energy barrier. (c) Heterogeneous formation of a hemispherical nucleus at a foreign substrate.

negative and varies as the cube of r, while the second term is positive and varying as r^2. As shown in Figure 6b, the sum of the two terms has a maximum that occurs when $d\Delta g/dr = 0$. The value of r at this point can be found by taking the derivative of (8b) and setting it equal to zero. This is known as the critical radius, r_c, and is given by:

$$r_c = 2\Omega\alpha/\Delta\mu \tag{9a}$$

$$= 2\Omega\alpha/kT\sigma \tag{9b}$$

The same analysis can be performed for heterogeneous nucleation, i.e., nucleation at a foreign surface. There are now two interfacial energies to consider, one between the crystal and solution and the other between the crystal and the substrate, as illustrated in Figure 6c. If we assume, for simplicity, that the nucleus is a hemisphere of radius r, we have:

$$\Delta g = -\{[(2/3)\pi r^3]/\Omega\}\Delta\mu + \pi r^2(2\alpha_{lc} + \alpha_{sc} - \alpha_{ls}) \tag{10}$$

where the subscripts "sc", "lc", and "ls" refer to substrate-crystal, liquid-crystal, and liquid-substrate respectively. The new expression for r_c becomes:

$$r_c = 2\Omega\alpha'/k_B T\sigma \tag{11a}$$

$$\alpha' = \alpha_{lc}\{1-(\alpha_{ls} - \alpha_{sc})/2\alpha_{lc}\} \tag{11b}$$

The term in the brackets is always less than one, provided the free energy of the crystal-substrate interface is less than that of the substrate-liquid interface. Thus the value of r_c at the substrate is reduced below that for nucleation in free solution. Figure 7 shows an example of the control over nucleation by surface structure in case of calcite nucleation on alkane thiol self-assembled monolayers.

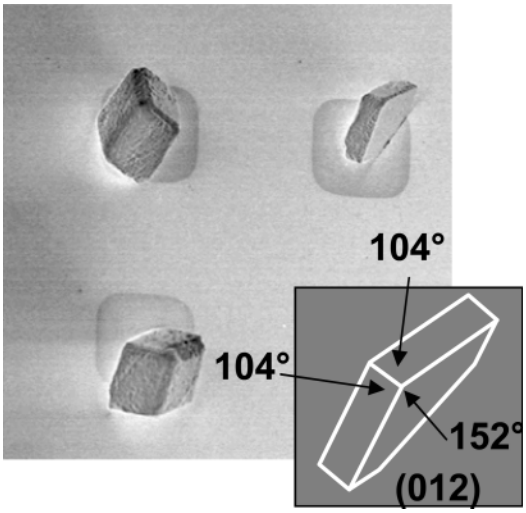

Figure 7. Nucleation of calcite on a template. The substrate consists of gold-coated mica which has been patterned with mercaptohexadecanoic acid (MHA)—a carboxyl terminated alkane thiol—using a micro-stamping method. The surrounding region was then coated with octadecane thiol. The crystals all nucleated on the MHA terminated regions and almost always with the (012) face as the plane of nucleation.

Nucleation pathways and Ostwald's Law of phases

If a solution is supersaturated, then regardless of the critical size or the presence of a foreign surface, the solution will eventually crystallize. What is significant about the critical size is that it controls the probability of a nucleus forming on any given timescale. In other words, it determines the kinetics of nucleation. To understand and quantify this, again consider Figure 6b. It shows that along with a critical nucleus size comes a nucleation barrier whose magnitude, Δg_n can be determined by substituting (9b) or (11a) into (8b) to get:

$$\Delta g_n = (16/3)\pi\alpha^3(\Omega/k_B T\sigma)^2 \tag{12a}$$

$$\propto \alpha^3/\sigma^2 \tag{12b}$$

It is this barrier that determines the kinetics of nucleation. As with any kinetically-limited chemical process, the nucleation probability is proportional to the exponential of the barrier height divided by $k_B T$. Thus the nucleation rate (Neilsen 1964; Abraham 1974) is given by:

$$J_n = A\exp(-\Delta g_n/k_B T) \tag{13}$$

where A is a factor that depends on many parameters. Substituting in the expression for Δg_n from (12) gives:

$$J_n = A\exp(-B\alpha^3/\sigma^2) \tag{14}$$

where we have grouped all of the factors other than interfacial energy and supersaturation into the coefficient B. Equation (14) shows just how strongly the nucleation rate depends on the supersaturation and the interfacial energy. They come in as the 2nd and 3rd powers respectively in the argument of an exponential! Figure 8 illustrates how strongly this function varies with supersaturation by showing the reciprocal of J_n, which is a measure of the induction time until nucleation at any given supersaturation.

An inherent assumption in the above discussion is that the pathway of nucleation goes directly from the solution to the formation of nuclei with ordered crystalline structure identical to that of the eventual bulk crystal. When the main concepts concerning equilibrium between large and small phases and the generation of nuclei of a new phase from an old were introduced by J.W. Gibbs, he was careful to point out that the composition of the "globulae," as he called them (i.e., the nuclei), would likely differ

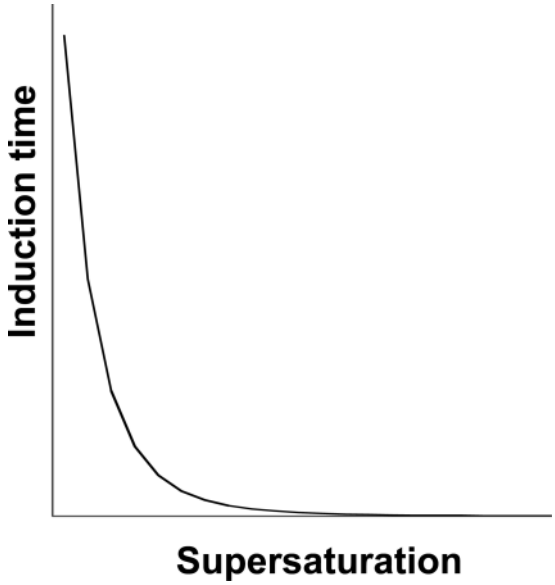

Figure 8. The induction time for nucleation is a strong function of supersaturation.

from the composition of a large sample of the new phase (i.e., the bulk) (Gibbs 1876, 1878). Since the surface tension of the "globulae," the main factor that determines the height of the barrier for nucleation, is not necessarily related to the surface tension of the interface between bulk samples of the two phases and cannot be measured independently, Gibbs stated that surface tension should be viewed as an adjustable parameter.

In further developments, some of the Gibbs's assumptions regarding the thermodynamics of nucleation of a fluid phase were transferred to the nucleation of ordered solids, such as crystals, from dilute or condensed fluids or from other solid states (Katz and Ostermier 1967; Neilsen 1967; Kahlweit 1969; Walton 1969). The classical nucleation theory emerged, in which the so called "capillary approximation" was widely used. In application to crystals, the approximation means that the molecular arrangement in a crystal's embryo is identical to that in a large crystal and hence, the surface free energy of the nuclei will equal the one of the crystal interface. However, there are many instances in which this is unlikely to be the case, simply because the energy barrier leading to a more disordered, less stable state is less than the one leading to the most stable state. This is the basis of the Ostwald-Lussac law of phases, which maintains that the pathway to the final crystalline state will pass through all less stable states in order of increasing stability (Nancollas 1982). If this law were strictly true, then, for example, the crystallization of $CaCO_3$ at room temperature from a pure solution would proceed by nucleation of amorphous material, which would then transform into vaterite, then aragonite, and finally calcite. Indeed, new evidence shows some calcitic biominerals begin as an amorphous calcium carbonate precursor that later transforms to its lower energy crystalline counterpart (Addadi et al. 2003).

Whether or not the Ostwald-Lussac law generally holds is unknown, as nucleation events are so difficult to study, both because they occur spontaneously and because the critical nucleus size is very small, typically in the 1 to 100 nm range. Nonetheless, one can construct a reasonable physical basis for the law. Taking Equation (14) as the rate of nucleation of a given phase, the only way a less stable phase can nucleate more rapidly than the most stable phase is if α^3/σ^2 is reduced by nucleating the less stable phase. But to say that this phase is less stable implies that the K_{sp} is larger, which in turn implies that σ is smaller. This means that, in order for the ratio α^3/σ^2 to become smaller, α must be reduced by an even greater factor for the less stable phase. Recall that α is proportional to

the difference between the change in free energy in forming a crystal with a surface (Δg) and that of forming an infinite crystal (Δg_b). In fact, starting with Equations (8a) and (8b), we have

$$\alpha = (\Delta g - \Delta g_b)/4\pi r^2 \quad (15a)$$

$$= \Delta g_s/4\pi r^2 \quad (15b)$$

The free energy terms, Δg_i, are themselves comprised of two terms: the change in enthalpy, Δh_i, and the change in entropy, Δs_i, i.e., $\Delta g_i = \Delta h_i - T\Delta s_i$). Now let's examine each of the terms. The statement that a phase is less stable is equivalent to one stating that Δg_b is smaller. That this should be so makes sense because the poorer bonding of the more disordered phase ensures that Δh_b will be smaller for its formation, and the higher level of disorder has the same impact on Δs_b, as illustrated in Figure 9. Therefore, the only way that α can become smaller is for the total change of free energy to decrease by even more, i.e., Δg_s must decrease as well. Equation (15b) reflects this. As with the bulk, since the surface of the less stable phase is likely to be more disordered than the surface of the most stable phase, both Δh_s and Δs_s are likely to be smaller. Nonetheless, this is not a proof, and the Ostwald-Lussac law of phases should only be viewed as a guiding principle rather than a statement of fact.

The nucleus shape

Equations (8)–(14) above were derived under the assumption of a spherical shape of the nucleus. If the nucleus has any other shape, obviously, the coefficients included in the parameters A and B in Equation (14) will take different values, but the overall conclusions on nucleation kinetics, it appears, will not change significantly. There is an important caveat in the latter statement, and it is in the assumption that we have a means to predict the nucleus shape in advance. In some cases, this is indeed so. Thus, thinking of a fluid phase nucleating within another fluid, Gibbs suggested that the shape of the nuclei is the one ensuring the lowest free energy of the nuclei, i.e., the sphere (Gibbs 1876, 1878). Accounting for crystal anisotropy and applying the free energy minimization selection criterion, one comes up with cubic or other faceted shapes and only slight modifications to Equations (8)–(14).

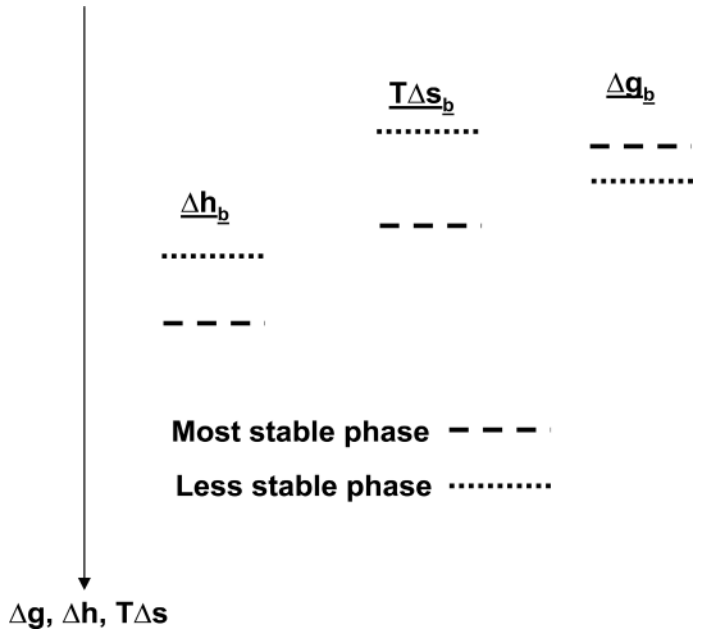

Figure 9. Schematic illustrating the relative contributions of enthalpy and entropy changes to the free energy change upon crystallization into the most stable and a less stable phase.

However, free energy minimization is not an absolute criterion for nucleus shape selection. In the simple model system considered by Gibbs, minimal free energy of the nucleus provides for a minimal free energy barrier for nucleation and, hence, for a nucleation pathway of fastest kinetics. Thinking of formation of structured crystalline nuclei, one is forced to realize that the one-dimensional picture, with the nucleus size as the only variable, is perhaps oversimplified. The free energy landscape then appears as a surface in a multi-dimensional space. In this space, multiple pathways exist between the initial state, that of single molecules suspended in the solvent, and the final state, crystals of sizes larger than the critical that grow, driven by $\Delta\mu$. Obviously, the observed rate of nucleation depends on the pathway that was selected or, in other words, we only see the products of the fastest nucleation pathway. Thus, we come up with a more general criterion for nucleus shape selection—which ensures the fastest nucleation rate.

With this in mind, one can understand the two experimental observations of crystalline nuclei that have yielded shapes far from the expected compact, smooth and polyhedral. It was found that the nuclei of the protein apoferritin are raft-like and consist of several rows of molecules in a single crystalline layer as shown in Figure 10 (Yau and Vekilov 2000, 2001). Obviously, due to the low number of intermolecular contacts this shape has a free energy significantly higher than a conceivable compact shape. However, it was found that for this protein, the formation of intermolecular contacts is significantly hampered (Chen and Vekilov 2002; Petsev et al. 2003) by a free energy barrier linked to the water structuring around the polar surface residues (see Figs. 11 and 12) (Petsev and Vekilov 2000a,b). It has been suggested that the quasi-planar shape ensures faster

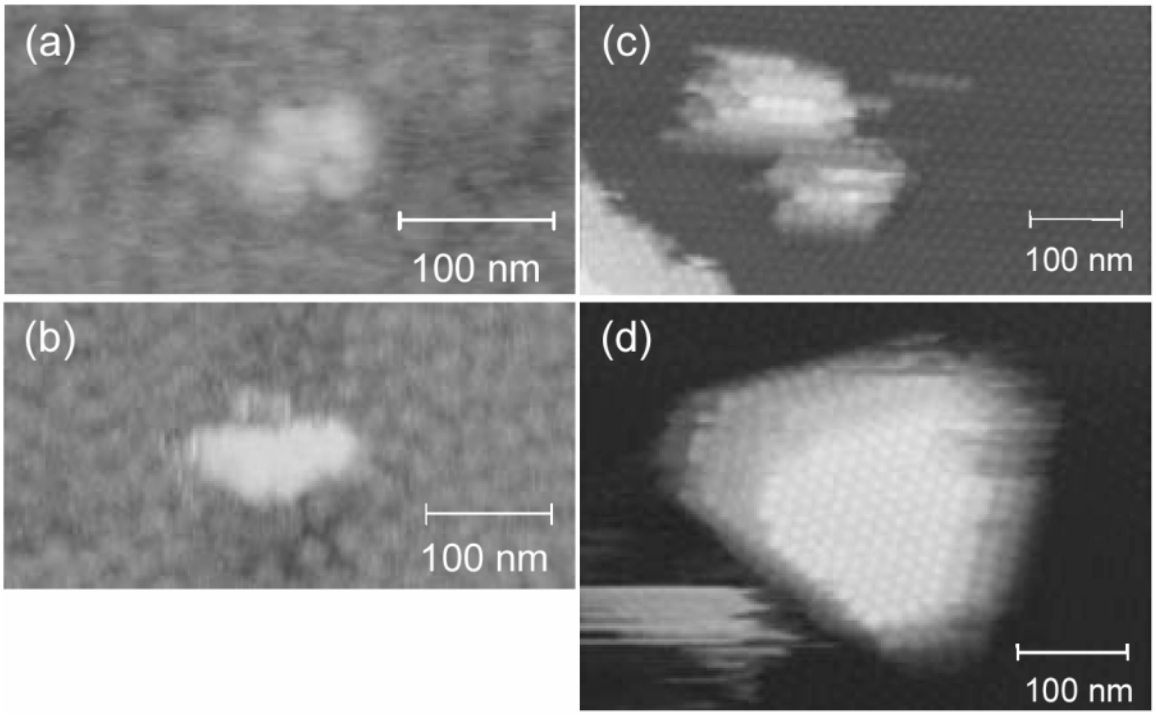

Figure 10. AFM images of sub-critical, near-critical clusters, and super-critical crystallites in the nucleation pathway of the apoferritin crystals. (a) A cluster consisting of two molecules with apoferritin concentration, C = 0.23 mg/mL and σ = 2.3. (b) A cluster consisting of six molecules in two rods with four and two molecules in each of the rods with C = 0.04 mg/mL and σ = 0.5. In both (a) and (b), the clusters have landed on the bottom of an AFM cell covered with a single layer of apoferritin molecules. (c) A near critical cluster that has landed on the (111) face of a apoferritin crystal at σ = 1.1. (d) A crystallite of ~ 150–180 molecules on a large crystal at σ = 1.1.

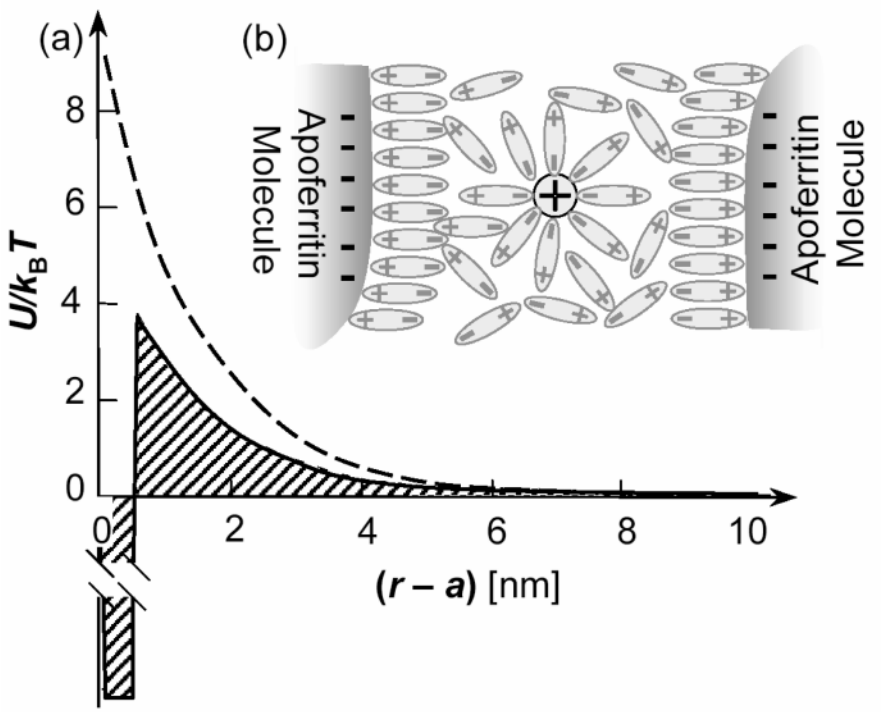

Figure 11. (a) The potential of pair interactions between apoferritin molecules. *Dashed line*: in the presence of $[Na^+] = 0.20$ M according to a hydration force model. *Solid line*: schematic representation of the interaction potential after the addition of Cd^{2+}. (b) Schematic representation of the build-up of counterions at the surface of the protein molecules that leads to the hydration repulsion reflected in (a).

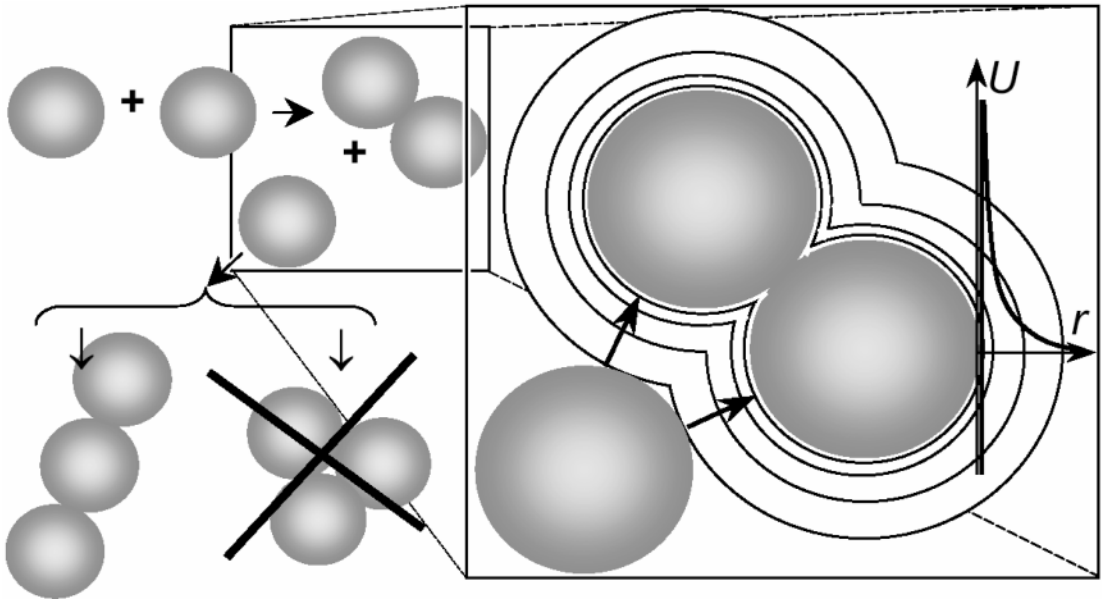

Figure 12. Schematic of formation of a trimer of molecules with an interaction potential consisting of long-range repulsion and short-range attraction, highlighted on $U(r)$ plot at far right. Contours around zoomed-in dimer represent repulsive potential lines in the plane of the image.

kinetics of nucleation because of the low number of intermolecular contacts that have to form and the low number of barriers that have to be overcome (Vekilov and Chernov 2002). Note that the presence of similar free energy barriers for the formation of crystalline contacts cannot be excluded for any material crystallizing from solution. Hence, non-equilibrium nucleus shapes maybe the rule, rather than the exception, for solution-grown crystals.

Another example of nucleus visualization comes from studies of a crystallizing suspension of colloid particles in a specially selected organic solvent (Gasser et al. 2001). At the relatively low supersaturations involved, the nuclei were quite large, consisting of around 100 particles, and had the shape of oblate ellipsoids. This shape deviates from the expected sphere and the surface was found to be rough, with many protrusions of three or four particles. The surface roughness is associated with high surface free energy, and a likely explanation for its presence is that it facilitates the attachment of particles to the nucleus and in this way contributes to faster kinetics of nucleation.

Crystal growth kinetics

Figure 13a schematically illustrates atomic processes occurring at a crystal surface. The surface consists of flat regions called terraces and raised partial layers called steps (Chernov 1961, 1984, 1989). The steps themselves are also incomplete, containing kinks. The kink sites are very important because molecules that attach there make more bonds to neighboring molecules than the ones that attach to the terraces or to flat step edges. Consequently they are more likely to stick. Conversely, when molecules leave the crystal, they can do so more easily by detaching from kinks than from either complete step edges

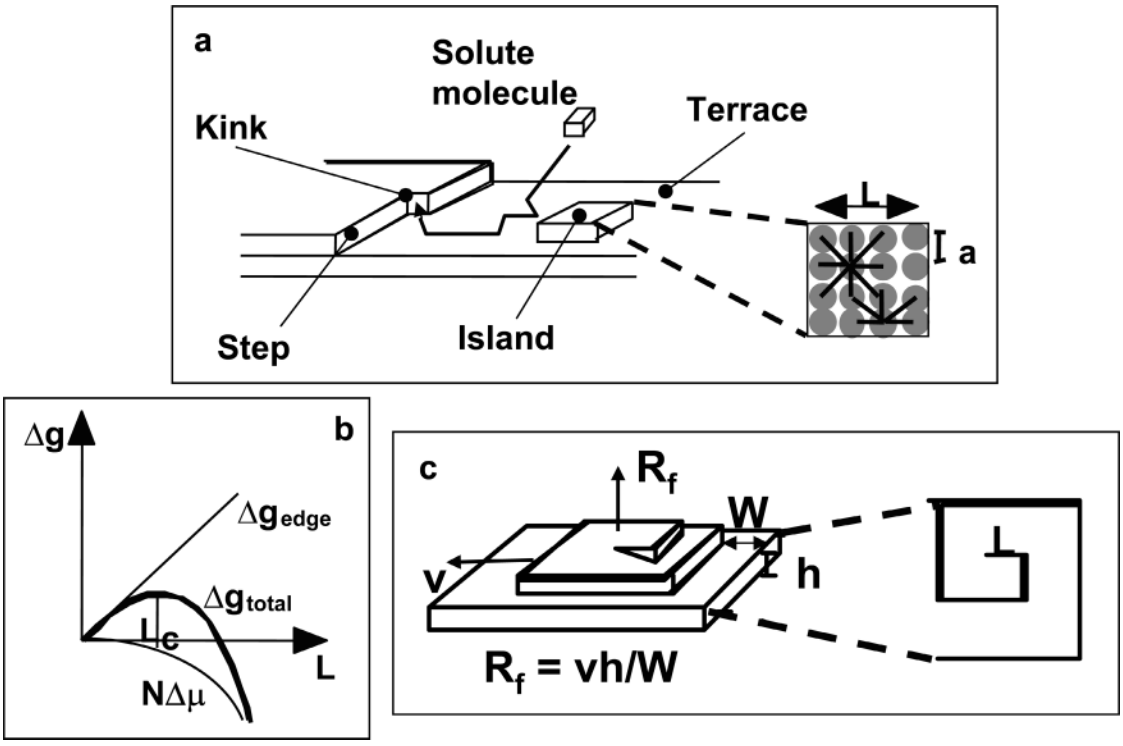

Figure 13. (a) Illustration of the atomic processes during crystal growth. Solute molecules enter kinks either directly from solution or after adsorbing and diffusing across terraces. Islands can nucleate on the terraces provided they overcome the free energy barrier to 2D nucleation illustrated in (b). (c) shows the geometry of a dislocation hillock. The existence of a critical size leads to the formation of the spiral structure, since the new segment of the step cannot move until it reaches that size.

or from embedded sites in the terraces. As a result, the rate at which molecules can be added to a crystal, for a given solute concentration, scales with the kink density. This means that the growth rates of crystals can be altered by either blocking kink sites or by roughening steps. We will come back to this later.

Even at equilibrium, the steps have kinks due to thermally activated detachment of molecules from the steps onto either the step edges or the terraces or even back into solution (Frenkel 1932; Burton et al. 1951; Chernov 1984). Consequently the step edges are not static; molecules are constantly attaching and detaching, even at equilibrium (Williams and Bartelt 1991; Barabasi and Stanley 1996). Figure 14a shows an example of a step edge at high resolution showing how this process makes the edge "fuzzy." If the crystal has weak bonds in all directions (think of non-interacting colloids as an extreme example), the step is perfectly rough and has an equilibrium kink density of about 1/2, i.e., every other site is a kink. Of course in most crystals, the bonds are anisotropic with some strong and some weak. The strengths of the bonds and the anisotropy in bonding determine the equilibrium kink density. For example, if a crystal possesses strong bonds parallel to a step edge but weak bonds perpendicular to the edge, the energy penalty for creating kinks is large, and the step will have a low kink density. If the converse is true, then the energy penalty is small, and the step will have a high kink density. All other factors being equal, these two types of steps will advance at very different rates. Figure 14b shows an example of steps on a crystal that has high anisotropy in bonding and exhibits rough steps in one direction and smooth steps in the other. Not surprisingly, at

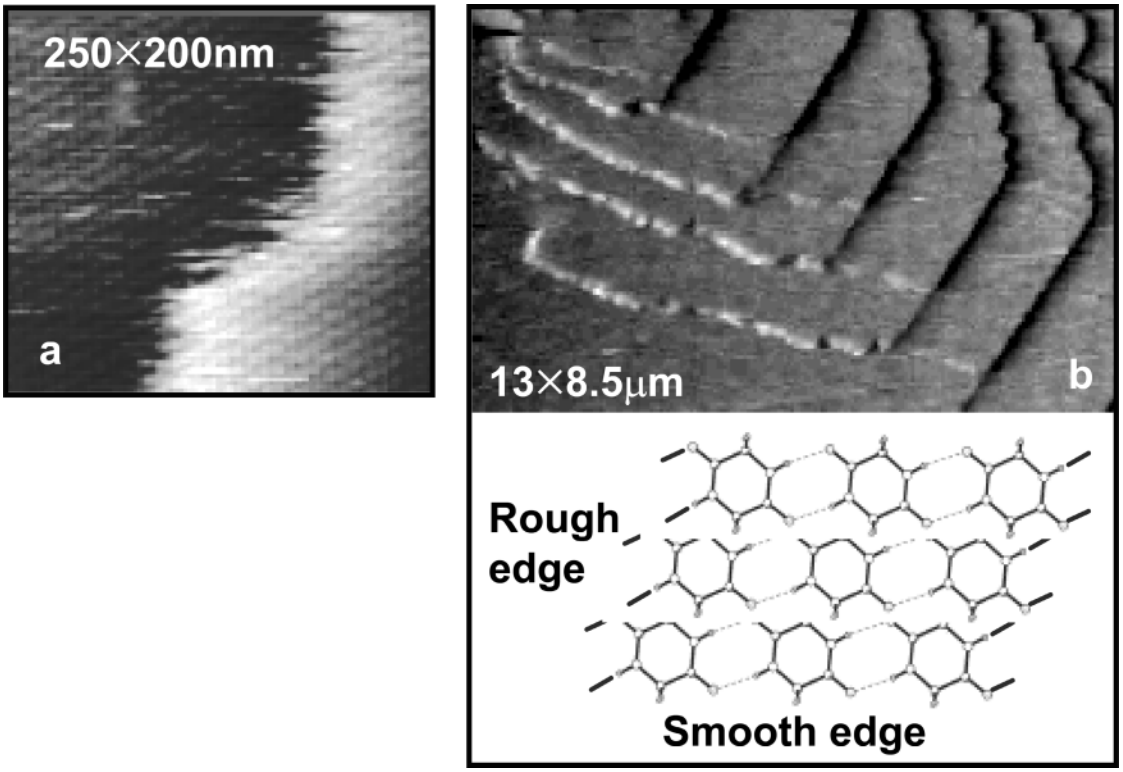

Figure 14. AFM images of (a) a step on a crystal of the protein canavalin showing the fuzziness of the step due to attachment and detachment of molecules, and (b) two types of steps on the surface of a glycine derivative of diketopiperazine (Gly-DKP) along with the packing geometry of the Gly-DKP molecules. The strong amine bonds along one axis and weak inter-ring bonds perpendicular to the plane of the rings leads to smooth steps along the strong-bonding direction and rough steps along the other.

the same supersaturation, the rate at which the rough step advances is ten times the rate for the smooth steps.

Growth from a supersaturated solution occurs because the flux of molecules attaching to the crystal surface exceeds the flux of molecules detaching from the surface. The probability that a molecule will detach from the crystal is solely determined by the strength of its bonds to its neighbors. Since the strength of bonding is a function of temperature rather than the flux to the surface, the total flux from the surface is nearly independent of concentration. In contrast, the flux to the surface is proportional to the bathing concentration. The solubility is then the concentration at which the two fluxes are equal. This raises an important aspect of crystal growth kinetics. Since the flux of molecules to the surface depends on the actual solute concentration (or activity), then, other factors being equal, highly soluble crystals will grow faster than sparingly soluble crystals, *even at equivalent supersaturations*. Shifting the solubility automatically changes the growth kinetics, providing yet another means of altering crystal growth rates (Davis et al. 2000).

The kinetics of the attachment and detachment processes at step edges are determined by the energy barriers seen by the molecules. It has been suggested that the barrier to desolvation, i.e., the breaking of bonds to solvent molecules, is the dominant barrier to attachment of a solute molecule to the step (Chernov 1961, 1984). While the basic idea that the solvation water is a major part of the barrier seems to have withstood the tests of time, recent simulations and modeling have modified the original scenario. Thus molecular dynamics simulations have shown that the life time of the hydrogen bonds in the structured water layer on the surface of protein molecules is of the order of nanoseconds (Makarov et al. 2000, 2002)—many orders of magnitude shorter than the characteristic time scales of the molecular attachment. In other words, the bonds between solvent molecules are broken and restored many times while a molecule is *en route* to an incorporation site, and the breaking of such a bond cannot be the rate-limiting stage. While an exact picture of the rearrangement of the water structure upon incorporation is still missing, there is significant evidence that the kinetic barrier is related to the energy characteristics of this rearrangement, and the rate of molecular attachment is determined by its rate (Petsev et al. 2003).

Clearly, all processes related to the solvent structure are influenced by solution composition. In particular, pH and ionic strength strongly influence step advancement rates. As an example, the dependence of step advancement rates on solute concentration at three different pH values for crystals of the protein canavalin is shown in Figure 15 (Land et al. 1997).

The primary barrier to detaching a molecule from a step are its bonds to adjacent molecules in the crystal. These barriers are difficult to influence just by altering solution composition because they are controlled by the crystal itself. However, introduction of impurities that incorporate into the crystal at sufficiently high concentrations can alter these detachment rates. As an example, Figure 16 shows the dependence of step advancement rates on Ca^{2+} activity for calcite grown in the presence of magnesium (Davis et al. 2000). With increasing magnesium levels, the activity at which the step speed goes to zero moves to higher values, i.e., the solubility increases, and, as discussed above, the solubility is a direct measure of equilibrium detachment rates.

The equations that govern growth kinetics depend on many assumptions about the pathways of mass transfer, but a very general set of considerations leads to some useful results. Since growth occurs on steps, for now we will ignore the source of the steps and just analyze the step kinetics. We will assume that the steps are rough and that the

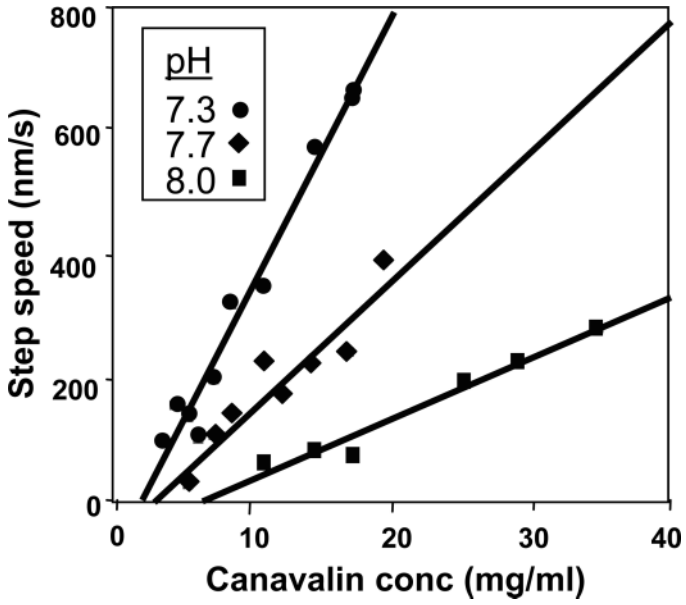

Figure 15. Dependence of step speed on concentration as a function of pH for the protein canavalin (From Land et al. 1997 with permission of Elsevier).

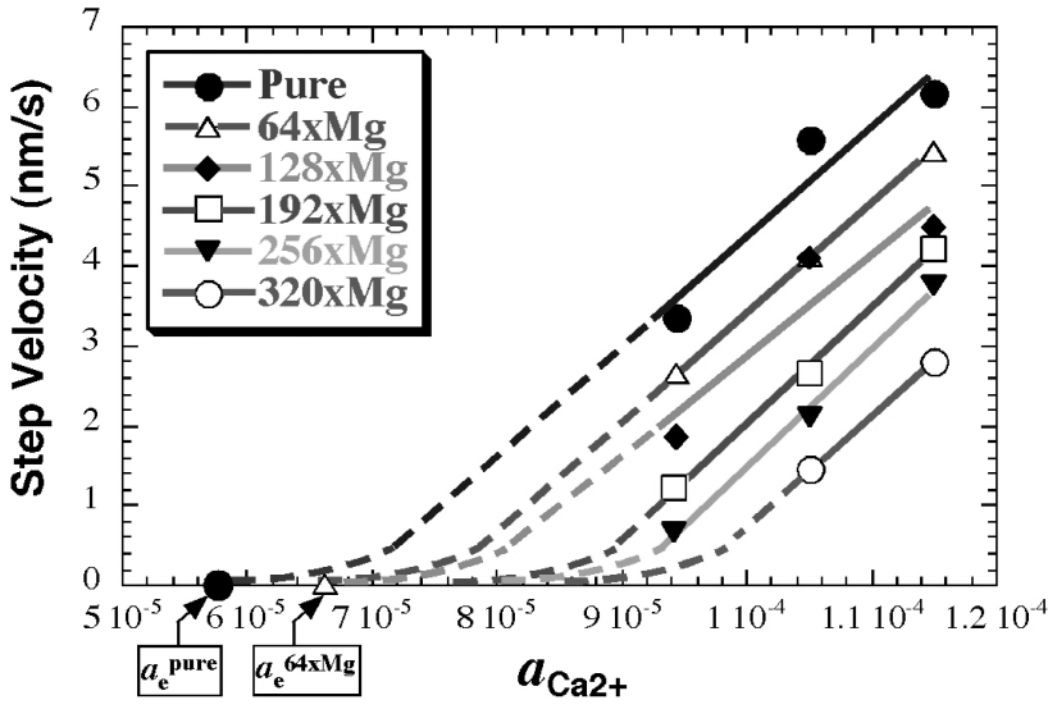

Figure 16. Measured dependence of step velocity on Ca^{2+}, activity, a_{Ca2+} as a function of Mg^{2+} concentration. The solubility shifts to higher activities, while the kinetic coefficient remains roughly constant. The solution activity of magnesium is expressed in a shorthand form where 320×Mg = 4.81×10^{-4} M (Modified after Davis et al. 2000).

concentration and activity are equal. The step advancement rate, R_s, is given by the difference between the attachment rate, R_a and detachment rate, R_d, (in numbers of molecules per unit of time). The step speed is just $R_s b$ where b is the depth of a kink (units of length). The attachment rate is given by the flux, F, of molecules to the step, times the area, ch, of a site on the step, times the probability of attachment, P_a, where c is the distance between molecules along the step and h is the step height. The detachment

rate from any given site is the attempt frequency, ν, times the probability of detachment, P_d. In the case of attachment, we will assume that the attachment probability is controlled by the interaction with the surrounding solvent and ignore site-to-site differences. However, because different kinds of sites have very different detachment rates, we must sum over the detachment probabilities for each type of site. The step speed becomes:

$$v/b = R_a - R_d \tag{16c}$$

$$= chFP_a - \nu \Sigma n_i P_{d,i} \tag{16b}$$

The flux is proportional to the concentration, and the detachment probability for a given site is $\exp(-E_i/kT)$. Equation (16) becomes:

$$v/b = chBC - \nu \Sigma n_i \exp(-E_i/kT) \tag{17}$$

where B is a concentration-independent coefficient that contains geometric factors, temperature, and mass terms describing the dynamics of solute diffusion near the surface. Also, in the rough step limit, the second term is independent of concentration. At equilibrium v is zero and $C = C_e$; consequently, we can replace the detachment term with $chBC_e$. Now the step speed becomes:

$$v = cbhB(C - C_e) \tag{18a}$$

$$= \Omega\beta(C - C_e) \tag{18b}$$

where Ω is the volume per molecule. The parameter β is commonly referred to as the kinetic coefficient (Chernov 1961, 1984). Table 1 gives derived kinetic coefficients for a number of crystal systems and shows that it has an inverse scaling with molecular size (Land and De Yoreo 1999; Vekilov 2003).

The above expression for the rate of the step propagation as the product of molecular size, kink density and net flux into a kink has been subjected to critical tests. Not surprisingly—it is essentially a reformulation of the mass preservation law—it was found to be exactly followed during growth of ferritin and apoferritin crystals (Yau et al. 2000a,b; Chen and Vekilov 2002; Petsev et al. 2003).

Table 1. Measured kinetic coefficients normalized by molecular size

System	β (*cm/s*)	b(Å) [c]	β/b (*rows/s*)
Calcite	0.3–0.5	3.2	$0.9–2\times10^{7}$
KH_2PO_4	0.1–0.4	3.7	$2–8\times10^{6}$
CdI_2	9×10^{-3}	4.2	2.1×10^{5}
Brushite	1.8×10^{-2}	5.8	3.1×10^{5}
GlyDKP [a]	3×10^{-3}	3.98	7.5×10^{4}
canavalin	1.2×10^{-3}	83	1.4×10^{3}
thaumatin	2.4×10^{-4}	58.6	4.1×10^{2}
catalase	3.2×10^{-5}	87.8	3.6×10^{1}
STMV [b]	4×10^{-6}	160	2.5×10^{0}

Notes:

a glycine derivative of diketopiperazine

b Satellite Tobacco Mosaic Virus

c kink depth

Derivation of the step speed dependence on concentration under many different assumptions leads to a similar relationship, the difference lying in the physical parameters of which β is comprised. One important exception is in the case of smooth steps. Then the density of kink sites depends on concentration increasing as $(C/C_e)^{1/2}$ for sufficiently small σ and one can no longer replace the expression for the detachment rate with the equilibrium expression. Then Equation (18) becomes:

$$v = \Omega\, \beta[(C - C_e) - C_e f(n_1)] \tag{19}$$

where n_1 is the density of nucleated kinks on a step edge and the function $f(n_1)$ rises linearly at low σ and approaches a constant at high concentrations. In other words, the step speed is non-linear at low concentrations, but becomes linear at high concentrations and then just looks like the rough limit with a lateral offset, as shown in Figure 17. Note the similarity of v vs. C for the smooth limit to the data on calcite shown in Figure 16.

One of the important consequences of Equations (18) and (19) is that the step speed scales with the absolute supersaturation, not the actual supersaturation. This means that if two types of crystals are placed in solutions of the same supersaturation, the crystal that is more soluble will grow faster than the other, simply because there is a larger flux of molecules to the surface. In other words, *step speed scales with solubility* and one cannot assume that faster growth rates imply faster kinetics at the kink sites.

Step generation: 2D nucleation vs. growth at dislocations

So far we have assumed that steps are pre-existing on a crystal surface. But without a new source of steps, any pre-existing steps would rapidly grow out to the edge of the crystal leaving a featureless terrace and no source for growth (For a demonstration of this phenomenon see Rashkovich 1991). One way to generate new steps is to generate two-dimensional islands of molecules that then spread outward (see Fig. 13a). But as in the case of three-dimensional nucleation, there is a critical size and a free energy barrier associated with this process, although in this case they are due to the excess free energy of creation of the new step edge rather than creation of a new surface (see Fig. 13b). (We will derive the equivalent 2D nucleation expressions later.) As Figure 18 shows, at sufficiently high supersaturations, crystal surfaces do grow from solutions by this mechanism (Teng et al. 2000; Land et al. 1997; Land and De Yoreo 1999). (Table 2

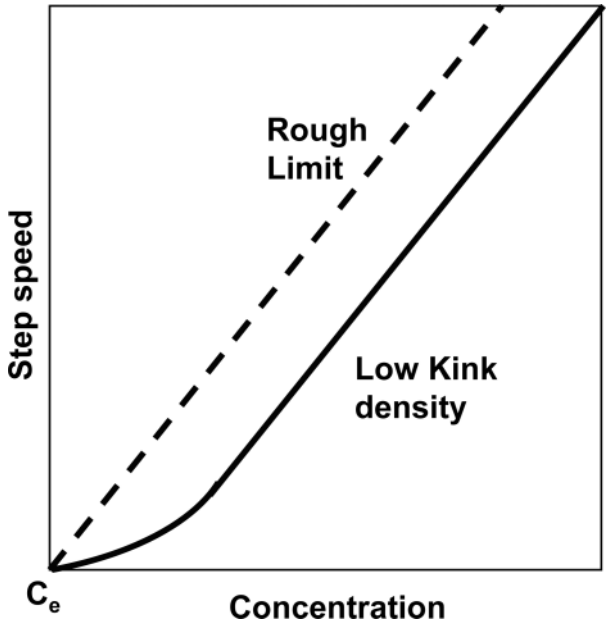

Figure 17. Dependence of step speed on concentration in the rough limit (Eqn. 18) and when steps are smooth due to low kink density (Eqn. 19).

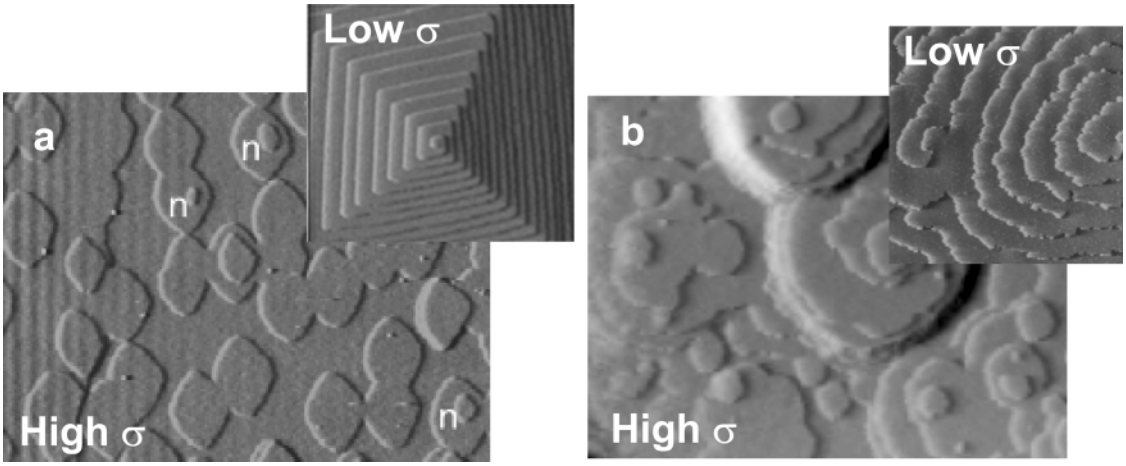

Figure 18. AFM images showing examples of 2D nucleation at high supersaturation for (a) calcite and (b) canavalin. N - locations where islands have nucleated on top of other islands.

Table 2. Measured step edge energies and critical sizes

System	$\gamma \cdot a$ *(ergs)* [a]	σ_{2D} [b]	N_c [c]
KH_2PO_4	4.2×10^{-14}	$\sigma\geq0.1$	650
Catalase	4.2×10^{-14}	$\sigma<0.2$	<2000
Thaumatin	1.3×10^{-13}	$\sigma\geq0.2$	800
$CaCO_3$	1.3×10^{-12}	$\sigma<3$	<600
Canavalin	1.5×10^{-12}	$\sigma\geq2.5$	800

Notes:

a where *a* equals the lattice spacing

b the supersaturation at which 2D nucleation was observed.

c number of molecules in the critical island at σ_{2D}

shows the supersaturation at which 2D nucleation is observed and the critical size at that supersaturation, based on measured step edge energies.) But at low supersaturations, the critical size is large and the probability of achieving it becomes prohibitively small. As an example, the critical island size for KH_2PO_4—the canonical solution-grown crystal—at an absolute supersaturation of 5% is about 10 nm or roughly 10,000 KH_2PO_4 molecules. The odds of obtaining an island of this size through a fluctuation that moves up a free energy gradient are understandably small. (In fact, when nucleation theory was applied to the growth of crystal surfaces back in the 1950's, researchers quickly realized that at the low supersaturations often used in crystal growth, 2D nucleation could never account for the observed growth rates.)

Fortunately, crystals are not perfect. They contain dislocations, i.e., breaks in the crystal lattice that generate permanent sources of steps (Frank 1949). Figure 13c shows a schematic of a step generated at a dislocation, and Figure 19 shows some examples of dislocation growth sources on crystal surfaces. Of course one is immediately struck by the fact that all of these sources generate spiral arrangements of steps. These features are referred to as dislocation spirals or dislocation hillocks or just growth hillocks. Besides the step speed, which we discussed above, the characteristics of the growth spiral are the distance between steps (i.e., terrace width) and shape. The terrace width, W is important in determining the growth rate, R_f, of a crystal face. As Figure 13c shows, R_f is equal to

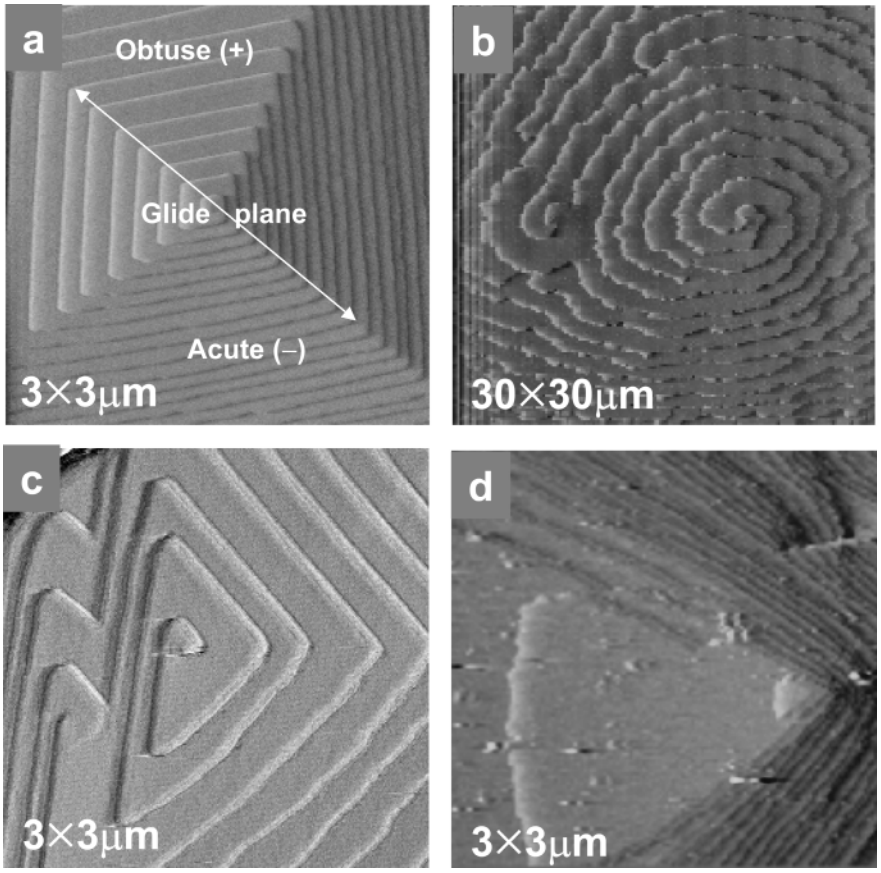

Figure 19. AFM images of dislocation hillocks on (a) calcite, (b) canavalin (c) brushite and (d) calcium oxalate monohydrate.

the hillock slope, p, times the step speed, v. But the hillock slope is just h/W where h is the step height, which is fixed by the crystal structure. So controls on terrace width are also important factors in determining growth rates (Burton et al. 1951).

To quantify growth on dislocation hillocks, we use the example of calcite (Teng et al. 1998, 2000). Growth of calcite on the {104} faces occurs on 3.1 Å monomolecular steps generated by dislocations. The advance of these steps leads to the formation of polygonal growth hillocks with steps parallel to the $<4\bar{8}1>$ and $<\bar{4}41>$ directions as illustrated in Figure 19a. The presence of a c-glide plane generates two distinct pairs of crystallographically identical steps denoted as the positive and negative steps due to the angles that the step risers make with the terraces (Paquette and Reeder 1995). The terrace widths of the two step types, $W_{\pm}$ are related to the step speeds, $v_{\pm}$ through $W_+/W_- = v_+/v_-$.

The birth of a new spiral segment is shown in Figure 20. If this new step segment remains in equilibrium with the adjacent reservoir of growth units, then it will only advance when the change in free energy, Δg, associated with the addition of a new row of growth units is negative. Taking into account the anisotropy in calcite step structure, one can show that Δg for a straight step is:

$$\Delta g_{\pm} = -(L/b)\Delta\mu + 2c\langle\gamma\rangle_{\pm} \quad (20a)$$

$$\langle\gamma\rangle_{+}=(1/4)[2(\gamma_{+}+\gamma_{-})+(\gamma_{++}+\gamma_{+-})] \quad (20b)$$

$$\langle\gamma\rangle_{-}=(1/4)[2(\gamma_{+}+\gamma_{-})+(\gamma_{--}+\gamma_{+-})] \quad (20c)$$

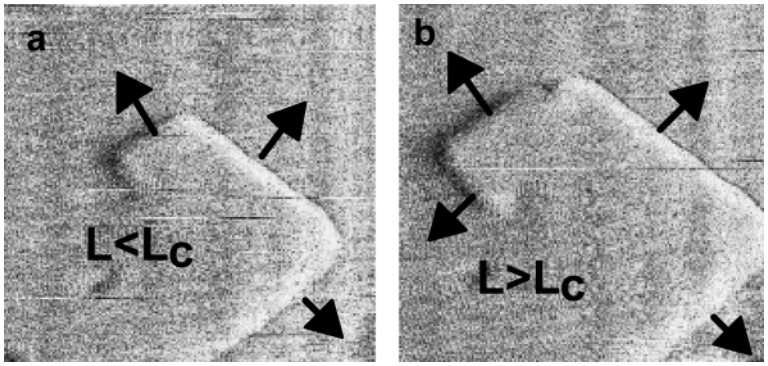

Figure 20. AFM images showing the birth of a new step segment on calcite. In (a), the smallest step is below the critical length and is not moving. In (b) it has exceed the critical length and begun to move. A new sub-critical step segment now appears. (Modified after Teng et al. 1998)

where L is the length of the step, b is the 6.4 Å intermolecular distance along the step, c is the 3.1 Å distance between rows, γ_+ and γ_- are the step edge free energies along the + and – steps, and γ_{++}, γ_{--} and γ_{+-} are contributions to the step edge free energy from the corner sites as illustrated in Figure 1c. (When step curvature is included, the terms on the right hand side of Eqns. 20b and 20c become integrals of $\gamma_\pm$ as a function of orientation.) Setting Δg to zero and substituting $kT\sigma$ for $\Delta\mu$ shows that free energy only decreases if the length of the step exceeds a critical value, L_c, given by:

$$L_{c\pm} = 2bc\langle\gamma\rangle_\pm / k_b T\sigma \tag{21}$$

Alternatively, setting $\Delta g = 0$ for a step of arbitrary length gives the length dependent equilibrium activity, $a_e(L)$:

$$a_e(L) = a_{e,\infty}\exp(2bc\langle\gamma\rangle/Lk_bT) \tag{22a}$$

$$= a_{e,\infty}\exp(\sigma L_c/L) \tag{22b}$$

where the subscript ∞ refers to the infinitely long step and a and $a_{e,\infty}$ are related by $a = a_{e,\infty}\exp(\sigma)$. Equations (22a) and (22b) are statements of the Gibbs-Thomson effect. It predicts that, even for the growth spiral, the critical length should scale inversely with the supersaturation as in Equation (21). Figure 21 shows that the results for calcite agree with the predicted dependence. The slopes of the lines give the values of $\langle\gamma\rangle_\pm$.

Figure 21 also shows that $L_{c\pm}$ vs. $1/\sigma$ exhibits a non-zero intercept. It marks the supersaturation, $\sigma_{c\pm}$ where $L_{c\pm}$ goes to zero. For $\sigma > \sigma_{c\pm}$, 1D nucleation along the step edge lowers the free energy of the steps. This supersaturation gives the approximate free energy barrier, $g_{1D\pm}$, to formation of a stable dimer on the step edge through $g_{1D\pm} = kT\sigma_{c\pm}$ (Chernov 1998).

The Gibbs-Thomson effect also affects step speeds for short step segments. Combining Equations (6), (18), and (22) leads to a length dependent step speed:

$$v_\pm(L) = v_{\pm\infty}\{1-[e^{(\sigma L_{c\pm}/L)}-1]/[e^\sigma-1]\} \tag{23}$$

where $v_{\pm\infty}$ is given by Equation (18) for $a_e(L\rightarrow\infty)$. When $\sigma << 1$, Equation (23) reduces to a commonly used approximation: $v = v_\infty(1-L_c/L)$ (Rashkovich, 1991). Unfortunately, in the few cases that have been investigated, the prediction of Equation (23) has turned out to be incorrect (See for example, Teng et al. 1998). Figure 22 shows the predicted dependence of v^+/v_∞ on L/L_c for calcite along with the measured dependence. The measured speed is independent of supersaturation or step direction and rises much more rapidly than that predicted by Equation (23).

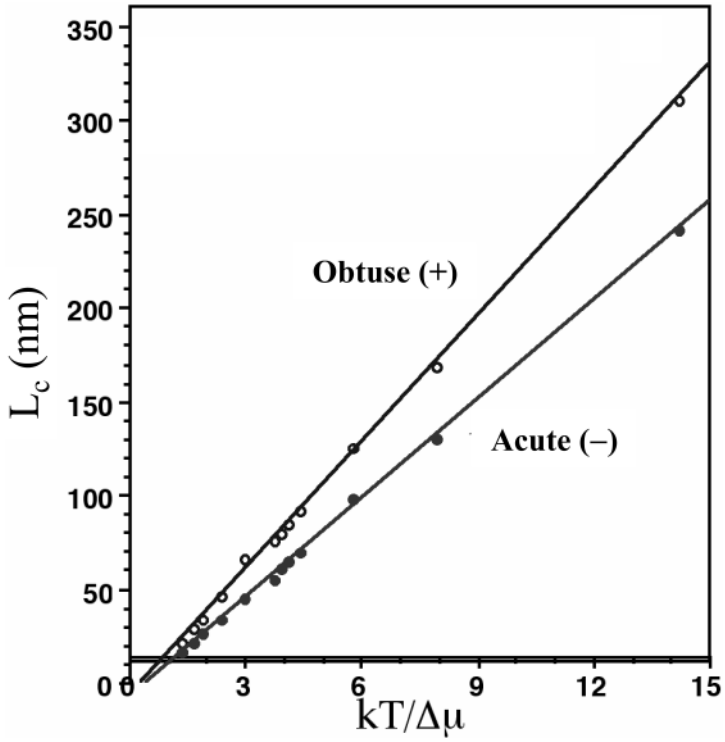

Figure 21. Dependence of critical length on supersaturation for calcite based on images like that in Figure 20. (Modified from Teng et al. 1998)

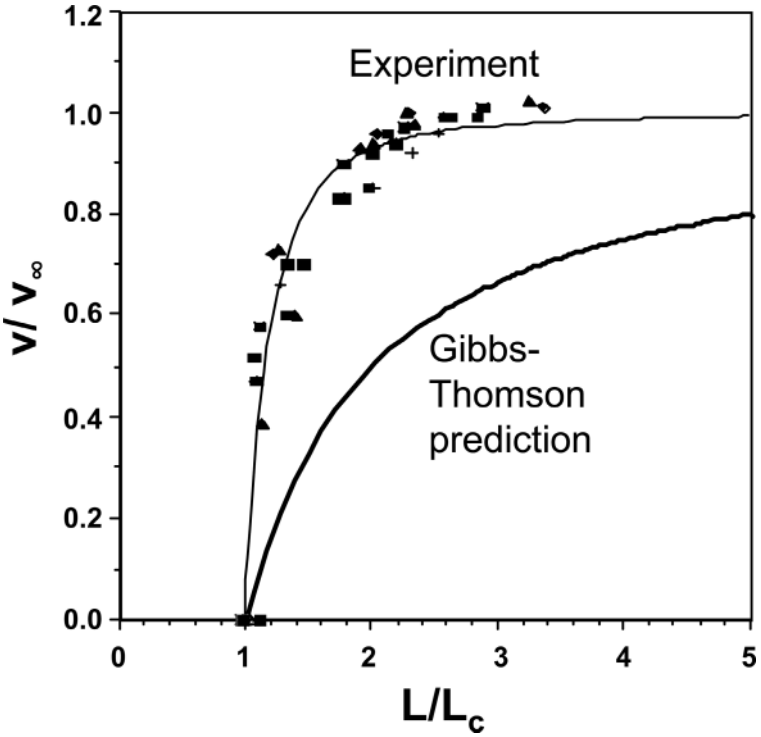

Figure 22. Dependence of step speed on step length for calcite showing the strong deviation from that expected based on the Gibbs-Thomson effect. (Modified from Teng et al. 1998)

Equation (23) was originally derived for spirals with isotropic step edge energies and kinetics, and assumes a high kink site density such that the rate of attachment is not limited by the availability of kinks. Voronkov (1973) proposed that for highly polygonized spirals, the distance between kink sites along a step is large so that the attachment rate is limited by their availability. He pointed out that the equilibrium shape of a step should be curved towards the corners and that the straight, central portion—which determines the speed—comprises only a small fraction of the step. (This prediction of step shape is verified in Fig. 20.) When the neighboring step advances, there is a rapid increase in the relative size of the straight portion and hence in the number of available kink sites. As a result, when L exceeds L_c, the step speed rises rapidly to its limiting value as its length increases from L_c to a length L' whose order of magnitude is given by $L_c + 2\Omega/ch\sigma$. Substituting in the constants of Ω, h and c specific to calcite (see Teng et al. 1998), we obtain $L'/L_c \sim 1.1$, a prediction which is consistent with the results in Figure 22. This result calls into question the use of data like those of Figure 21 to derive step edge energies by applying the Gibbs-Thomson formalism. Unfortunately, this is currently an unresolved area of crystal growth science.

Both the existence of a critical length and the length dependence of the step speed impact the terrace width and hence the growth rate. Consider an isotropic square spiral. If the step speed is zero for $L < L_c$ and jumps discontinuously to its maximum step speed, v_∞ at $L = L_c$, then the terrace width would be given by $4L_c$ (Burton et al. 1951; Rashkovich 1991). However, because the step speed rises gradually from zero to v_∞, the terrace width is larger by a factor that we will refer to as the Gibbs factor, G. Equation (23) leads to $G = 2.4$ for small σ, giving a terrace width of $9.6L_c$, which decreases to $G = 1$ in the limit of large σ.

For the rhombohedral spiral of calcite, the terrace widths for the two step directions become:

$$W_+ = 2G(1+B)\langle L_c\rangle/\sin\theta \tag{24a}$$

$$W_- = 2G(1+1/B)\langle L_c\rangle/\sin\theta \tag{24b}$$

where B is v^+/v^-, $\langle L_c\rangle$ is the average value of L_c for the two step directions and θ is the angle between adjacent turns of the spiral. Figure 23 shows the measured dependence of $W_\pm$ on σ as well as $W = 9.6\langle L_c\rangle$ obtained using Equation (24) at small σ. As predicted, the terrace widths scale inversely with σ, but due to the anomalously rapid rise in $v(L)$, the measured G factor is close to one. As a consequence, the growth rate of the calcite surface is about 2.5 times that predicted from classical growth theory (Burton et al. 1951; Chernov 1961).

MODIFYING THE SHAPES OF GROWTH HILLOCKS AND CRYSTALS

The shapes of crystals are controlled by a combination of energetic and kinetic factors (Burton et al. 1951; Chernov 1961). The equilibrium shape is that which minimizes the total surface free energy of the crystal, which is in turn the sum of the individual products of surface area times interfacial energy (see Fig. 24a). Thus low energy faces are preferentially expressed. On the other hand, crystal shape is rarely achieved by equilibration in a solution at equilibrium conditions, but rather during exposure to growth conditions. The slowest growing faces become the largest, and rapidly growing faces either become small or disappear altogether. Not surprisingly, the faces which are the low energy faces tend to also be those that grow slowly. Thus faces expressed during growth tend to be those expressed at equilibrium as well, although the sizes of the faces depend more critically on kinetic factors as well as the details of the

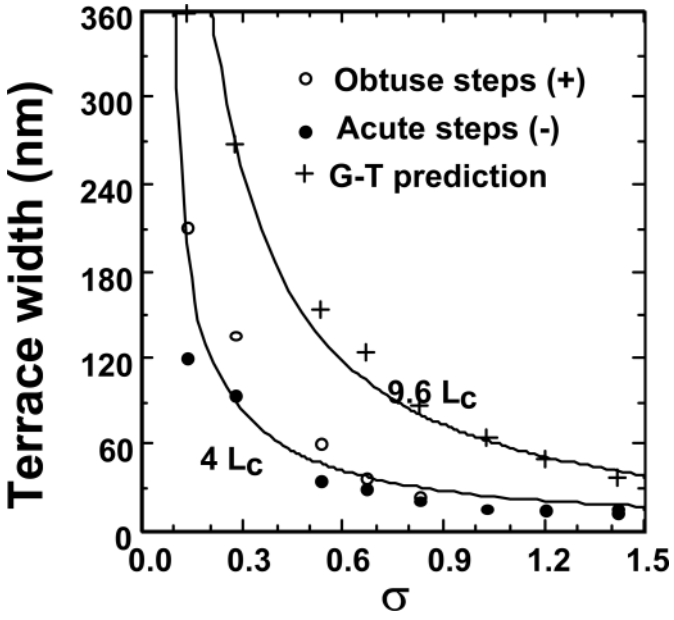

Figure 23. Dependence of terrace width on supersaturation on calcite. The solid and open symbols are the measured values. The solid line fit to those values is just four times the measured critical length. The crosses give the prediction using the Gibbs-Thomson equation and the fit is just 9.6 times the measured critical length. (Modified from Teng et al. 1998)

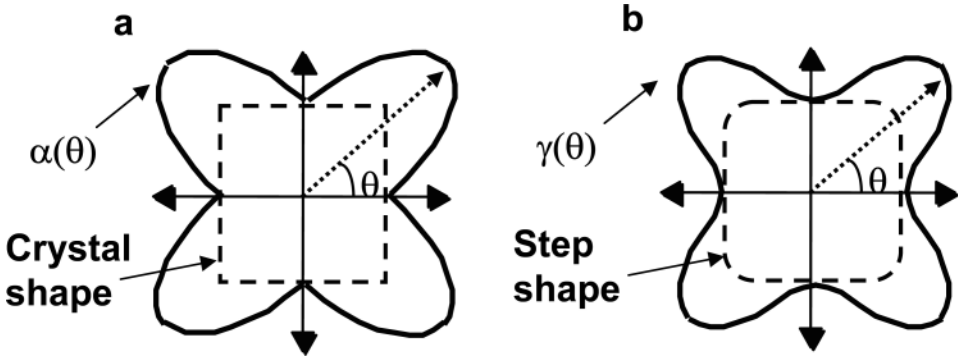

Figure 24. Schematic illustrating the relationship between (a) interfacial free energy and crystal shape, and (b) step edge free energy and step shape for simple cases.

growth sources, such as the number steps generated at a dislocation source. Because the chemical and structural factors that lead to low energy faces are also present at the step edges, the shapes of growth hillocks as well as the equilibrium shapes of the critical nucleus also tend to mimic the shapes of the growth faces, although, once again, kinetic factors lead to preferential expression of certain steps. Strictly speaking, the orientation dependence of the step edge energy, which is what determines the equilibrium step shape, is not the same as that of the surface energy in the same plane. For one thing, crystal facets are the result of true cusps in the dependence of surface energy on orientation, which is a 2D feature (Herring 1951; Chernov 1961). In contrast, while the minima in the dependence of step edge energy on orientation lead to the preferential expression of certain step directions, due to the presence of kinks, in 1D there are no true cusps (see Fig. 24b) (Chernov 1961, 1984). Calcite again provides an excellent example. As Figure 25 shows, the shape of the crystal face mimics the hillock shape, which in turn mimics the shape of the critical step segment.

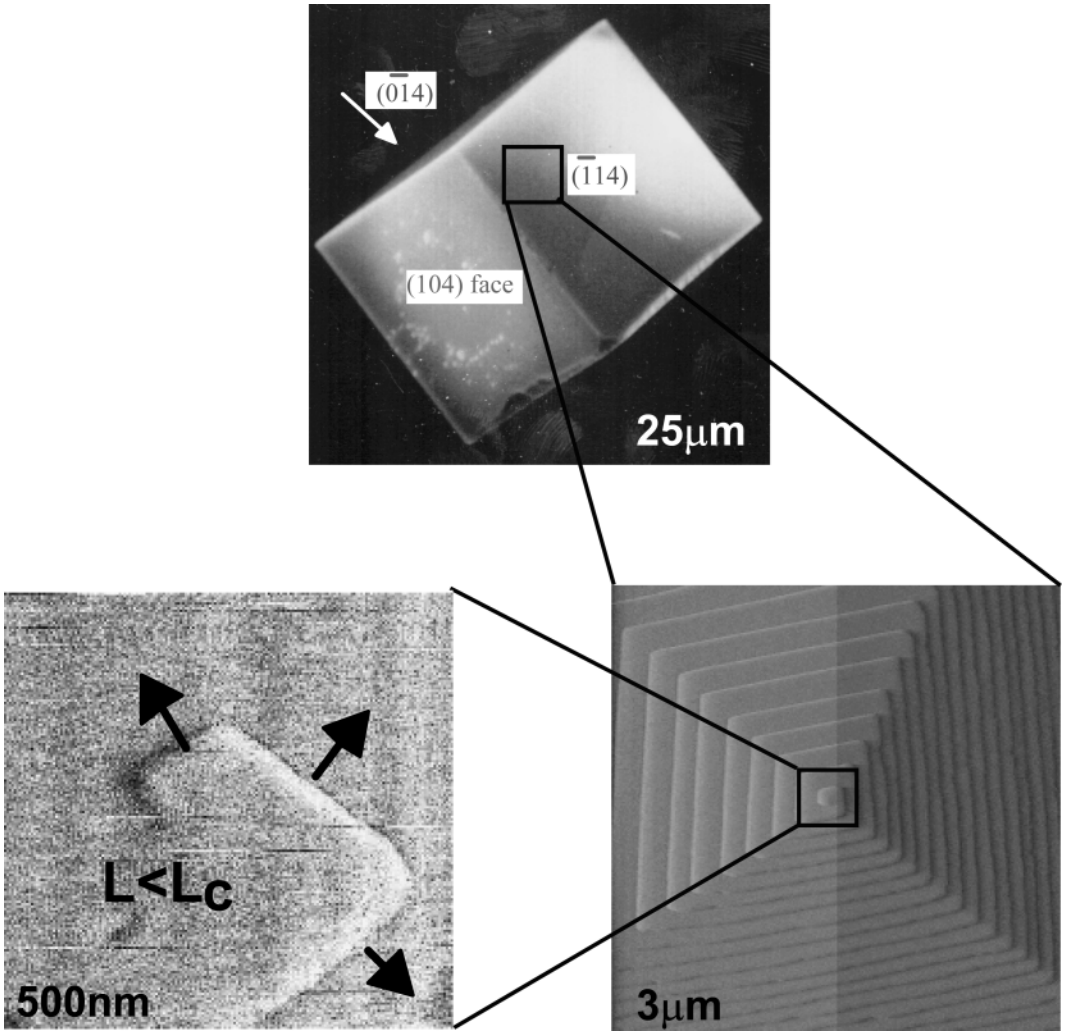

Figure 25. For many systems, there is a close similarity between step shape, hillock shape and facet shape. This example is from calcite.

As a result of these relationships, it is possible to modify the shapes of crystals by introducing ions or molecules that alter the shapes of growth hillocks through interactions with the step edges. These growth modifiers can be organic and include both peptides and large proteins, but even small inorganic modifiers may play a role in this process, given their presence in naturally occurring waters and cellular fluids (Weiner and Dove 2003). There are four mechanisms by which ions or molecules can modify growth hillocks, either by changing the step speed or by altering the step edge energy. They are: 1) step pinning, 2) incorporation, 3) kink blocking, and 4) step edge adsorption. Each of these major mechanisms for growth inhibition exhibits a characteristic dependence of step speed on supersaturation and impurity concentration as illustrated in Figure 26 (Dove et al. 2004).

1) Step pinning: Certain types of impurities block the attachment of molecules to the step edges (see Fig. 26a). The only way the step can continue to advance is by growing around those blocking sites (Cabrera and Vermileya 1958). As long as the average spacing between the impurities is much greater than the critical radius of curvature for the step, the step can continue to advance unimpeded. But when the spacing becomes comparable to the critical curvature, once again the Gibbs-Thomson effect

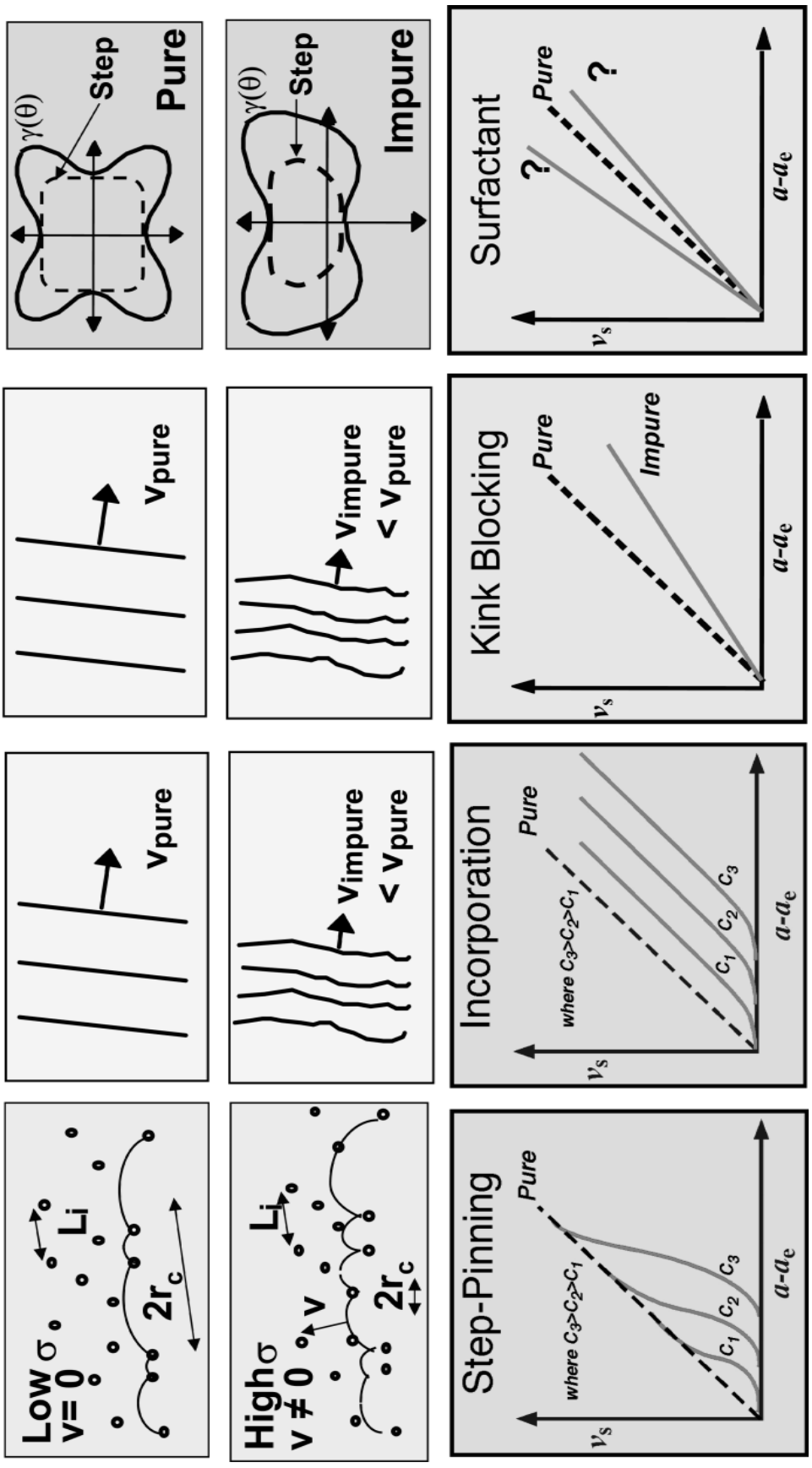

Figure 26. The four models for impurity interactions and their effect on step kinetics: (a) step pinning, (b) incorporation, (c) kink blocking, and (d) surfactant action (Dove et al. 2004).

influences growth. Moreover, if the average impurity spacing becomes so small that the step curvature must exceed the critical radius in order to pass between them, the step stops moving altogether. Although the step kinetics appear to be altered, this is actually a thermodynamic effect. It isn't the impurity *per se* that stops the step, but rather the fact that, according to the Gibbs-Thomson equation, the true supersaturation is a function of curvature and goes to zero at the critical curvature. If the radius of curvature should fall below r_c due, for example, to step fluctuations, the solution actually becomes undersaturated and the step retreats until the radius of curvature increases to r_c. In terms of supersaturation, for a given impurity content, there is a critical supersaturation, σ_d below which the crystal surface enters a so-called "dead zone" where no growth occurs (Cabrera and Vermileya 1958; Chernov 1961, 1984; Rashkovich 1991; Voronkov and Rashkovich 1994). As the supersaturation is increased, the crystal begins to grow with a speed given by Equation (23), with L_c and L replaced by r_c and r, eventually recovering the speed of the step in pure solution as shown in Figure 26a. Because the average impurity spacing decreases as the impurity level increases, the value of σ_d and width of the dead zone both become larger.

The relationship between σ_d and the impurity concentration can be derived by comparing the average impurity spacing with the critical radius (Cabrera and Vermileya 1958; Potapenko 1993; van Enckevort and van der Berg 1998). If the solution impurity concentration is C_i, then the surface density is $n_i = \Gamma C_i$ where Γ is derived from the Langmuir isotherm for the impurity. The average impurity spacing is equal to $1/(\kappa n_i^{0.5})$ where κ is a number of order unity that depends on the lattice geometry. Equating this to twice the critical radius at σ_d leads to:

$$1/(\kappa n_i^{0.5}) = 2r_c = 2\Omega\alpha/kT\sigma_d \qquad 25a$$

Rearranging gives the result that $\sigma_d \propto C_i^{0.5}$. Specifically,

$$\sigma_d = (2\kappa\Omega\alpha)n_i^{0.5} = (2\kappa\Gamma\Omega\alpha)C_i^{0.5} \qquad 25b$$

$$\sigma_d \propto C_i^{0.5} \qquad 25c$$

Interestingly, one example for which the data clearly demonstrates this square root dependence is the growth of ice in the presence of antifreeze proteins. Other systems spectacularly fail to display this behavior. In some cases, the reason for the discrepancy is clear (Land et al. 1999), while in other highly relevant cases for biomineralization, such as calcite growing in the presence of Sr^{3+}, the source of the observed anomalous dependence is unknown (Wilson et al. 2002).

Step pinning is highly dependent upon the details of the impurity-step interactions. Consequently, the same impurities that may block one type of step can leave steps on adjacent faces—or even other types of steps on the same face—unimpeded. In this way step pinning generally leads to a change in hillock and crystal shape (For examples, see De Yoreo et al. 2002 and Qiu et al. 2003). Figure 27 shows the example of the growth of calcium oxalate monohydrate (COM), the main mineral forming phase of kidney stones, in the presence of citrate, a naturally occurring modulator of stone formation (Qiu et al. 2003). The images were collected in the regime just above σ_d. Citrate has no effect on the {010} face but dramatically slows growth on the $\{\bar{1}01\}$ face. In fact, one particular step (the [101]) is most strongly affected. In pure solution, its speed is more than an order of magnitude higher than that of the adjacent [120] steps. But at the citrate level used in this experiment, it slows by a factor of 12 and loses lateral stability, while the <120> steps only slow by a factor of two and becomes rough and rounded. The result is that the step speed on that face is nearly isotropic, and the hillocks become rounded. The crystal shape reflects these changes. Crystals become rounded plates with large $\{\bar{1}01\}$ faces. Molecular

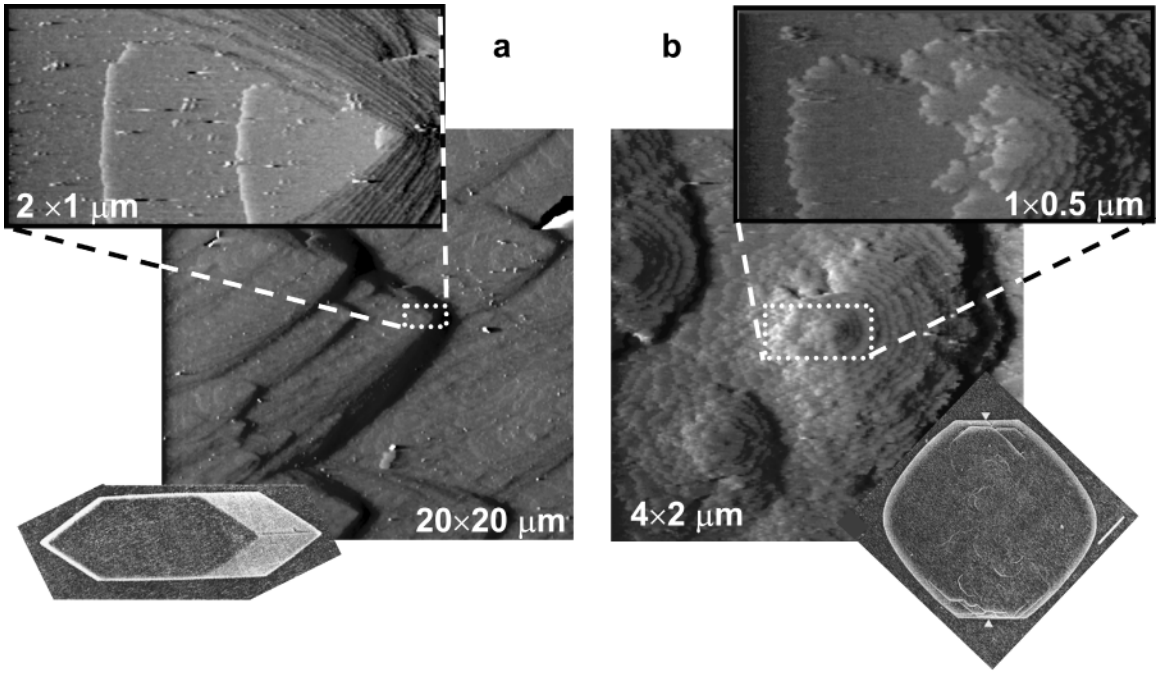

Figure 27. Example of a system that exhibits step pinning. AFM images of growth hillocks on calcium oxalate monohydrate growing (a) pure solution and (b) solution containing sodium citrate. The lower insets show the resulting crystal morphologies.

simulations provide an explanation for these observations by predicting citrate-step binding energies that scale with the observed impacts on step propagation. The naturally occurring protein osteopontin has the inverse effect: it pins steps on the {010} face but not the $\{\bar{1}01\}$ face. In combination, the two modifiers can poison growth on both sets of faces.

2) Incorporation: Impurity incorporation occurs when foreign ions or molecules become captured by advancing steps or otherwise incorporate at kink sites along a step edge to become part of the growing crystal. Typically the impurity molecules distort the crystal structure, thereby increasing the internal energy of the solid through an enthalpic contribution (van Enckevort and van der Berg 1998; Davis et al. 2000). The resulting increase in free energy is manifested as an increase in the solubility (K_{sp}) of the crystal, leading to a lower effective supersaturation. Since σ is defined as the natural logarithm of the ion activity product divided by the solubility constant, an increase in the solubility of the crystal reduces the effective supersaturation (σ_{eff}). As shown in Figure 26b, this result shifts step velocity curves to higher equilibrium activities, resulting in what appears as a dead zone at low supersaturation ($\sigma<\sigma_d$). But this is a misinterpretation, because the supersaturation needs to be recalculated using the value of K_{sp} for the impurity-bearing phase. Above σ_d, the linear relationship between step velocity and concentration characteristic of the pure system is regained. However, the absolute magnitude of the step velocity always remains below that of the pure system at the same supersaturation. Moreover the slope of v versus C remains unchanged. Recalling from Equation (18) that dv/dC gives the kinetic coefficient, β this implies that there is no impact on kinetics of attachment processes at the step edges. The example of Mg incorporation in calcite was shown in Figure 16.

There is an important caveat to discuss here. Incorporation does not have to result in decreasing growth rates and can even increase the growth rate at sufficiently low impurity concentrations. This is because the incorporation of the impurity *always* increases the entropy of the solid, making it more stable and decreasing its solubility

(Astilleros et al. 2002). This type of behavior is seen for low Sr concentrations in calcite (Wilson et al. 2003).

Incorporation mechanisms can also change crystal shape. In particular, when the impurities incorporate at different rates into adjacent steps, the result is a crystal with sharp changes in impurity content near the boundaries of the two step directions (e.g., the positive and negative step directions in calcite). Those spatial variations lead to strain near the boundary, which lowers the supersaturation and inhibits growth. In calcite grown with Mg, this effect has been proposed as the source of crystal elongation along the {001} axis (Davis et al. 2003).

3) Kink blocking: When impurities adsorb to kink sites for very short residence times, they lead to an effective reduction in kink site density (Bliznakow 1958; Chernov 1961), with or without incorporation. That is not to say that they permanently block step advancement at that site, just kink propagation. Thus there is no dead zone, and the solubility is unaffected. Instead, the kinetic coefficient—and hence the slope of v vs. C is reduced as shown in Figure 26c. As with step pinning, because this effect is highly dependent on specific impurity-step interactions, kink blocking can result in a change in crystal shape. Figure 28 shows an example of a system that appears to exhibit this behavior, though the only proof is the kinetic data presented in the figure, along with the observation that the steps, though roughened slightly, do not change shape.

4) Surfactants: Impurities that lower the interfacial energy by adsorbing to surfaces modify many aspects of the surface dynamics and are known as surfactants. Impurities that adsorb to step edges can have similar effects, modifying growth by lowering the step edge energy. Although there are a number of variants on this process, here we consider the end-member situation whereby the modification is a purely thermodynamic effect that changes the orientation dependence of the step edge energy, γ. As a result, the minimum energy step shape undergoes a transition to a new lowest energy form when the impurity concentration exceeds a threshold value. Figure 26d illustrates this evolution by a "2D Wulff construction" of step edge free energy for the case of a growth hillock that develops in a pure and impurity-modified system. The concepts behind this type of impurity modification were worked out for changes in 3D crystal shape due to true 2D surfactants (Hartman and Kern 1964; Kern 1969), but the extension to 1D is straightforward.

Evidence for this type of impurity effect comes from changes in microscopic (step edge direction) and macroscopic (expression of crystal facets) morphology in the absence of a kinetic effect. Indeed, impurity interactions by step edge adsorption are unique because step flow rates can exhibit little deviation from the pure system. As an example of this type of behavior, we again look to the calcite system. Figure 29 shows the effect of right-handed and left-handed aspartic acid on the shapes of growth hillocks and the resulting macroscopic crystals (Orme et al. 2001). The steps do not exhibit the pinning observed for citrate on COM, yet the shapes of the hillocks are dramatically altered. Moreover, the symmetry about the calcite glide plane is broken such that L-aspartic acid gives one chirality while D-aspartic acid gives the opposite chirality. There are new step directions that switch from one side of the glide plane to the other when the amino acid enantiomer is switched from L to D. These shapes were analyzed in terms of changes in step edge energetics with the modifier acting as a 1D surfactant. In fact, the overall reduction in terrace width demonstrates a true reduction in average step edge energy. But the relative degree to which the orientation dependence of step edge free energy is changed compared to the kinetic coefficient is unclear. What is clear from these experiments, however, is that, as in the case of COM with citrate and calcite with Mg, the overall shapes of the resulting crystals are being controlled by the shapes of the growth hillocks on existing faces.

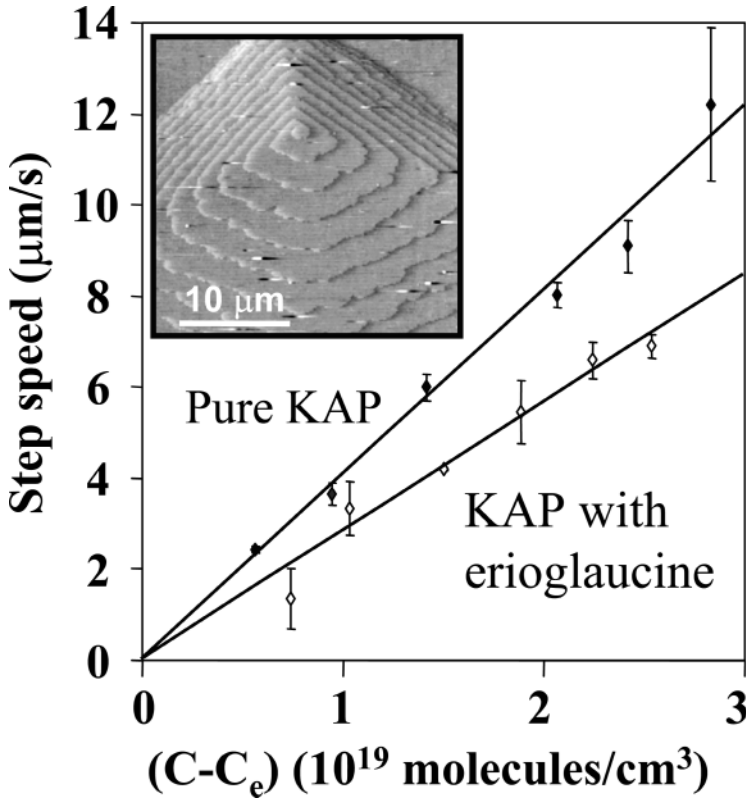

Figure 28. Example of system that exhibits behavior expected for kink blocking. AFM image and dependence of step speed on concentration for potassium acid phthalate with and without the organic dye, erioglaucine. The steps roughen slightly and the kinetic coefficient is reduced, but there is no dead zone, little or no shift in equilibrium solubility, and no change in shape.

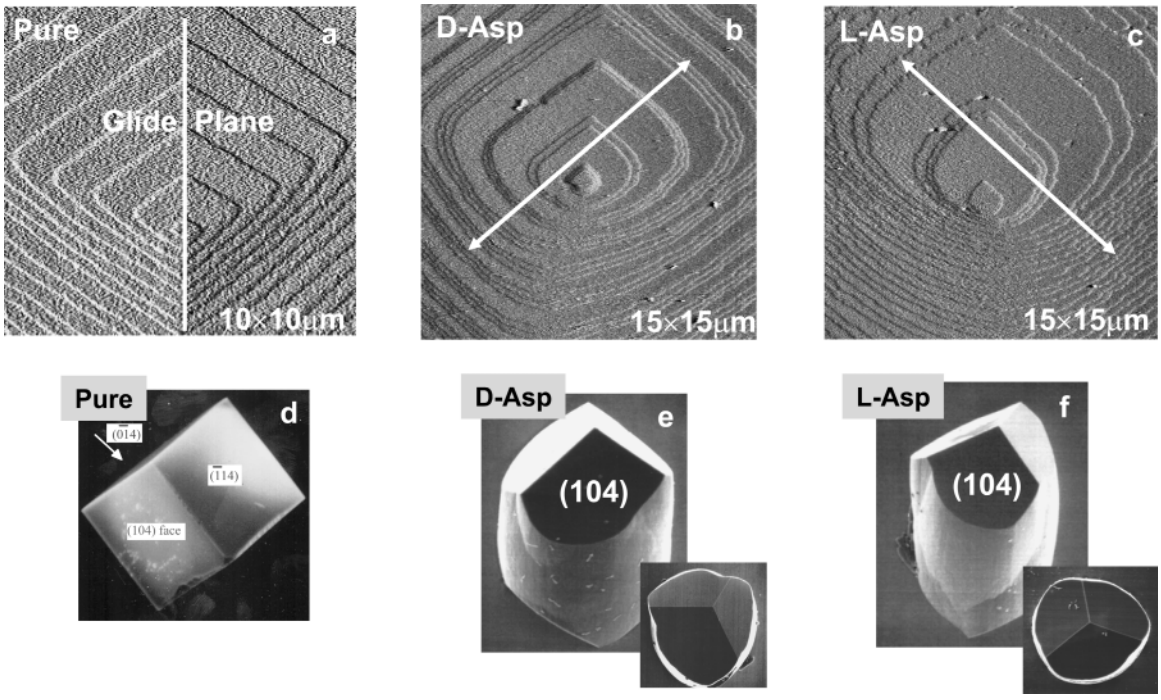

Figure 29. Example of system that exhibits behavior expected for addition of a surfactant. AFM images of calcite grown in (a) pure solution, (b) Solution containing D-aspartic acid and (c) solution containing L-aspartic acid. The shape changes dramatically and even shows a left-right shape dependence that corresponds to that of the additive. (d-f) show that the resulting crystal shape reflects these changes. (After Orme et al. 2001).

CONCLUSION

The physical processes of nucleation and crystal growth are inherent to the biological process of mineralization. Deciphering the control mechanisms exerted by organisms over nucleation and growth is one of the central challenges facing us as we try to understand how biominerals are formed. The concept of the energy landscape, though quite detached from the biology, provides a framework for relating the interactions between the controlling agents and the physical changes in shape, structure, and phase, regardless of whether those agents act as members of solid molecular scaffolds or ions in solutions. In this chapter, we have attempted to show how the principles of crystallization relate to these physical properties.

The single most important concept for understanding nucleation is that of the critical size and its relationship to the main external control parameter, the supersaturation, and the primary materials control parameter, the interfacial energy. Most importantly, the magnitude of the interfacial energy depends on the atomic-scale at the interface and, consequently, surfaces can be used by organisms to control both the location and orientation of biominerals. Secondarily, the details of the free energy landscape that separates the solvated phase from the final bulk crystal has a large impact on the pathway of nucleation and its manipulation may allow organisms to precipitate inorganic compounds into an easily shaped but metastable amorphous phase, which is then driven to convert to the final crystalline phase. Unfortunately, while these concepts are based on a firm physical foundation, clear and quantifiable links to real systems have yet to be established.

Critical size and free energy barriers continue to be central concepts during the growth phase of crystals, but the potential mechanisms for controlling the process appear to be greater in number and diversity. The critical parameters continue to include supersaturation and free energy, but the free energy of the interface is supplanted by that of the step. Moreover, the kinetics of attachment and detachment become of equal importance in determining growth rates and crystal shapes. These processes are typically quantified by a single parameter, the kinetic coefficient, which unfortunately masks the physics behind solute incorporation. Surprisingly, while many processes including desolvation, adsorption, surface diffusion, chemical reaction, and eventual incorporation can, in principle, both impact this coefficient and depend on the details of system chemistry, AFM studies of recent years are pointing towards rearrangement of waters to allow the solute to access the surface as the dominant factor. Consequently, the kinetic coefficient shows a clear scaling with molecular size. Once size is taken into account, the apparent energy barrier to step motion is surprisingly similar for all systems analyzed.

Due to the combined importance of both the thermodynamics of the step edge and the kinetics of solute attachment and detachment, there are a number of opportunities for organisms to modulate the growth phase. Unlike the situation with nucleation of biominerals, a widely accepted model for shape modification has been developed based on the concept of stereochemical recognition. Within this model, the modulators of growth exhibit stereochemical recognition for otherwise unexpressed faces of the mineral. Attachment to those faces then stabilizes them, producing a new crystal habit. Proposed examples include calcium oxalate monohydrate with citrate, ice with anti-freeze glycoproteins, and calcite with inorganic impurities such as Li and Mg, as well as organic modifiers containing carboxyl groups such as aspartic acid, glutamic acid, and acidic peptides. In principle, this mechanism can and probably does occur for some systems. However, as shown in this chapter, many of the classic systems for which this model was proposed clearly display behavior better explained through specific impurity-step interactions on existing faces. The differences between these two models of shape

modification have yet to be reconciled and highlight an inescapable conclusion: While the past century has led to a deep understanding of the physical principles of nucleation and growth, we are far from understanding how living organisms utilize those principles to control the formation of biomineral structures.

ACKNOWLEDGMENTS

This work was performed under the auspices of the U.S. Department of Energy by the University of California, Lawrence Livermore National Laboratory under contract No. W-7405-Eng-48

REFERENCES

Abraham FF (1974) Homogeneous Nucleation Theory. Academic Press, New York

Addadi L, Moradian J, Shay E, Maroudas NG, Weiner S (1987) A chemical model for the cooperation of sulfates and carboxylates in calcite crystal nucleation: relevance to biomineralization. Proc Nat Acad Sci 84:2732-2736

Addadi L, Raz S, Weiner S (2003) Taking advantage of disorder: amorphous calcium carbonate and its roles in biomineralization. Adv Mat 15:959-970

Aizenberg J, Black AJ, Whitesides GM (1999a) Control of nucleation by patterned self-assembled monolayers. Nature 398:495-498

Aizenberg J, Black AJ, Whitesides GM (1999b) Oriented growth of calcite controlled by self-assembled monolayers of functionalized alkanethiols supported on gold and silver. J Am Chem Soc 121:4500

Aizenberg J, Grazul JL, Muller DA, Hamann DR (2003) Direct fabrication of large micropatterned single crystals. Science 299:1205-1208

Archibald DD, Qadri SB, Gaber BP (1996) Modified calcite deposition due to ultrathin organic films on silicon substrates. Langmuir 12:538–546

Astilleros JM, Pina CM, Fernndez-daz L, Putnis A (2002) Molecular-scale surface processes during the growth of calcite in the presence of manganese. Geochim Cosmochim Acta 66:3177-3189

Barabási A-L, Stanley EH (1995) Fractal Concepts in Surface Growth. Cambridge University Press, Cambridge

Berman A, Ahn DJ, Lio A, Salmeron M, Reichert A, Charych D (1995) Total alignment of calcite at acidic polydiacetylene films: Cooperativity at the organic-inorganic interface. Science 259:515-518

Binder K, Fratzl P (2001) Spinodal decomposition. *In*: Phase Transformation in Materials. Kostorz G (ed) Wiley, New York

Bliznakow G (1958) Crystal habit and adsorption of cosolutes. Fortsch Min 36:149

Burton WK, Cabrera N, Frank FC (1951) The growth of crystals and the equilibrium structure of their surfaces. Royal Soc London Philos Trans A243:299-358

Cabrera N, Vermileya DA (1958) Growth and Perfection of Crystals. John Wiley & Sons, New York; Chapman and Hall, London

Calvert P (1992) Biomimetic ceramics and composites. MRS Bulletin XVII:37-44

Chaikin PM, Lubensky TC (1995) Principles of condensed matter physics. Cambridge University Press, Cambridge

Chen K, Vekilov PG (2002) Evidence for the surface diffusion mechanism of solution crystallization from molecular-level observations with ferritin. Phys Rev E 66:21606

Chernov AA (1961) The spiral growth of crystals. Sov Phys Uspekhi 4:116-148

Chernov AA (1984) Modern Crystallography III: Crystal Growth. Springer, Berlin

Chernov AA (1989) Formation of crystals in solutions. Contemp Phys 30:251-276

Chernov AA (1998) Theoretical and Technological Aspects of Crystal Growth. *In*: Materials Science Forum. Fornari R, Paorichi C (eds) TransTech Publications, USA, p 71-78

Collins MJ, Westbroek P, Muyzer G, DeLeeuw JW (1992) Experimental evidence for condensation reactions between sugars and proteins in carbonate skeletons. Geochim Cosmochim Acta 56:1539-1544

Crenshaw MA (1972) The soluble matrix from Mercenaria mercenaria shell. *In*: International Symposium on Problems in Biomineralization. Schattauer FK (ed) Verlag, New York

Davis KJ, Dove PM, De Yoreo JJ (2000) Resolving the controversial role of Mg^2 in calcite biomineral formation. Science 290:1134-1137

Davis KJ, Dove PM, Wasylenki LE, De Yoreo JJ (2004) Morphological consequences of differential Mg^{2+} incorporation at structurally distinct steps on calcite. Am Min (in press)

DeYoreo JJ, Orme CA, Land TA (2001) Using atomic force microscopy to investigate solution crystal growth. *In*: Advances in crystal growth research. Sato K, Nakajima K, Furukawa Y (eds) Elsevier Science, New York, p 361-380

DeYoreo JJ (2001) Eight Years of AFM: What has it taught us about solution crystal growth., *In:* 13th International Conference on Crystal Growth. Hibiya T, Mullin JB, Uwaha M (eds) Elsevier, Kyoto, Japan

De Yoreo JJ, Burnham A, Whitman PK (2002) Developing KDP and DKDP crystals for the world's most powerful laser. Int Mat Rev 47:113-152

Dove PM, Davis KJ, DeYoreo (2004) Inhibition of $CaCO_3$ crystallization by small molecules: the magnesium example. *In:* Solid-Fluid Interfaces to Nanostructural Engineering, Vol. II. Liu XY, De Yoreo JJ (eds) Kluewer/Plenum Academic Press, New York (in press).

Dunitz JD (1994) The entropic cost of bound water in crystals and biomolecules. Nature 264:670-670

Fink DJ, Arnold IC, Heuer AH (1992) Eggshell mineralization: A case study of a bioprocessing strategy. MRS Bulletin XVII:27-31

Frank FC (1949) The influence of dislocations on crystal growth. Discussions Faraday Soc 5:48

Frenkel J (1932) Note on a relation between the speed of crystallization and viscosity. Phys J USSR 1:498-510

Gasser U, Weeks E, Schofield A, Pusey P, Weitz D (2001) Real-space imaging of nucleation and growth in colloidal crystallization. Science 292:258-262

Gibbs JW (1876) On the equilibrium of heterogeneous substances. Trans Connect Acad Sci 3:108-248

Gibbs JW (1878) On the equilibrium of heterogeneous substances. Trans Connect Acad Sci 16:343-524

Hartman P, Kern R (1964) Le changement de facies par adsorption et al theorie dea "PBC." Acad Sci Paris 258:4591-4593

Herring C (1951) The use of classical macroscopic concepts in surface tension problems. *In:* Collection: Structure and properties of solid surfaces. McGraw-Hill, New York, p 143

Heywood BR, Mann S (1994) Template-directed nucleation and growth of inorganic materials. Adv Mater 6:9-20

Hohenberg PC, Halperin BI (1977) Theory of dynamic critical phenomena. Rev Mod Phys 49:435-479

Johnson DA (1982) Some thermodynamic aspects of inorganic chemistry. Cambridge University Press, Cambridge

Kahlweit M (1969) Nucleation in Liquid solutions. *In*: Physical Chemistry, Vol. VII. Eyring H (ed) Academic Press, New York, p 675-698

Katz JL, Ostermier BJ (1967) Diffusion cloud chamber investigation of homogeneous nucleation. J Chem Phys 47:478-487

Katz EP, Li S (1973) The intermolecular space of reconstituted collagen fibrils. J Mol Biol 21:149-158

Kashchiev D (1999) Nucleation: Basic Theory with Applications. Butterworths, Heinemann, Oxford

Kashchiev D (2003) Thermodynamically consistent description of the work to form a nucleus of any size. J Chem Phys 118:1837-1851

Kern R (1969) Crystal growth and adsorption. *In*: Growth of Crystals. Sheftal' NN (ed) Consultants Bureau, New York, p 3-23

Lacmann R, Schmidt P (1977) Nucleation and equilibrium forms of mixed crystals. *In:* Current Topics in Materials Science 2. Kaldis E, Scheel HJ (eds) North–Holland, Amsterdam, p 301–325

Land TA, De Yoreo JJ, Lee JJ (1997) *In situ* AFM investigation of canavalin crystallization kinetics. Surf Sci 384:136

Land TA, De Yoreo JJ (1999) *In situ* AFM investigation of growth source activity on single crystals of canavalin. J Cryst Growth 208:623

Land TA, Martin TL, Potapenko S, Palmore GT, De Yoreo JJ (1999) Recovery of surfaces from impurity poisoning during crystal growth. Nature 399:442

Makarov VA, Andrews BK, Smith PA, Pettitt BM (2000) Residence times of water molecules in the hydration sites of myoglobin. Biophys J 79:2966-2974

Makarov VA, Pettitt BM, Feig M (2002) Solvation and hydration of proteins and nucleic acids: a theoretical view of simulation and experiment. Acc Chem Res 35:376-384

Mann S, Archibald DD, Didymus JM, Heywood BR, Meldrum FC, Wade VJ (1992) Biomineralization: Biomimetic potential at the inorganic-organic interface. MRS Bulletin XVII:32-36

Mann S (2001) Biomineralization: Principles and Concepts in Bioinorganic Materials Chemistry. Oxford University Press, New York

Miller A (1984) Collagen: The organic matrix of bone. Philos Trans R Soc London B 304:455-477

Mullin JW (1992) Crystallization, 3rd edition. Butterworths, Oxford

Mutaftschiev B (1993) Nucleation. *In:* Handbook on Crystal Growth. Hurle DTJ (ed) North–Holland, Amsterdam, p 187-248

Nancollas GH (ed) (1982) Biological Mineralization and Demineralization. Life Sciences Research Report. Springer-Verlag, New York

Neilsen AE (1964) Kinetics of Precipitation. Pergamon, Oxford

Neilsen AE (1967) Nucleation in aqueous solutions. *In:* Crystal Growth. Peiser S (ed) Pergamon, Oxford, p 419-426

Orme CA, Noy A, Wierzbicki A, McBride MY, Grantham M, Dove PM, DeYoreo JJ (2001) Selective binding of chiral amino acids to the atomic steps of calcite. Nature 411:775-779

Paquette J, Reeder RJ (1995) Relationship between surface structure, growth mechanism, and trace element incorporation in calcite. Geochim Cosmochim Acta 59:735-749

Petsev DN, Vekilov PG (2000a) Evidence for non-DLVO hydration interactions in solutions of the protein apoferritin. Phys Rev Lett 84:1339-1342

Petsev DN, Thomas BR, Yau S-T, Vekilov PG (2000b) Interactions and aggregation of apoferritin molecules in solution: Effects of added electrolytes. Biophysical J 78:2060-2069

Petsev DN, Chen K, Gliko O, Vekilov PG, (2003) Diffusion-limited kinetics of the solution-solid phase transition of molecular substances. Proc Natl Acad Sci USA, 100:792-796

Potapenko SY (1993) Moving of steps through an impurity fence. J Cryst Growth 133:147-154

Qiu SR, Wierzbicki A, Orme CA, Cody AM, Hoyer JR, Nancollas GH, Zepeda S, De Yoreo JJ (2003) Molecular Modulation of Calcium Oxalate Crystallization by Osteopontin and Citrate (submitted)

Rashkovich LN (1991) KDP Family of Crystals. Adam-Hilger, New York

Sikes CS, Yeung ML, Wheeler AP (1990) Inhibition of calcium carbonate and phosphate crystallization by peptides enriched in aspartic acid and phosphoserine. *In*: Surface Reactive Peptides and Polymers: Discovery and Commercialization. Sikes CS, Wheeler AP (eds) ACS Books, Washington, ch 5

Tanford C (1980) The hydrophobic effect: formation of micelles and biological membranes. John Wiley & Sons, New York

Teng H, Dove PM, Orme C, De Yoreo JJ (1998) Thermodynamics of calcite growth: Baseline for understanding biomineral formation. Science 282:724

Teng H, Dove PM, De Yoreo JJ (2000) Kinetics of calcite growth: Surface processes and relationships to macroscopic rate laws. Geochim Cosmochim Acta 64:2265

Travaille, AM, Donners JJM, Gerritsen, JW, Nico, NAJM, Nolte, RJM, van Kempen, H (2002) Aligned growth of calcite crystals on a self-assembled monolayer. Adv Mater 14:492-495

van Enckevort WJP, van der Berg ACJF (1998) Impurity blocking of crystal growth: a Monte Carlo study. J Cryst Growth 183:441–455

Vekilov PG, Feeling-Taylor AR, Yau S-T, Petsev DN (2002a) Solvent entropy contribution to the free energy of protein crystallization. Acta Crystallogr Section D 58:1611-1616

Vekilov PG, Feeling-Taylor AR, Petsev DN, Galkin O, Nagel RL, Hirsch RE (2002b) Intermolecular interactions nucleation and thermodynamics of crystallization of hemoglobin C. Biophys J 83:1147-1156

Vekilov PG, Chernov AA (2002) The physics of protein crystallization. *In*: Solid State Physics. Ehrenreich H, Spaepen F (eds) Academic Press, New York, p 1-147

Vekilov P (2003) Microscopic, mesoscopic, and macroscopic lengthscales in the kinetics of phase transformations with proteins. *In*: From Solid-Fluid Interfaces to Nanostructural Engineering. Vols. I and II. Liu XY, De Yoreo JJ (eds) Kluewer/Plenum Academic Press, New York

Voronkov, VV (1973) Dislocation mechanism of growth with a low kink density. Sov Phys Crystallogr 18:19-223

Voronkov VV, Rashkovich LN (1994) Step kinetics in the presence of mobile adsorbed impurity. J Cryst Growth 144:107-115

Wada K, Fujinuki T (1976) Biomineralization in bivalve mollusks with emphasis on the chemical composition of the extrapallial fluid. *In*: The Mechanisms of Mineralization in the Invertebrates and Plants. Watabe N, Wilbu KM (eds), Univ SC Press, Columbia, p 175-190

Walton AG (1969) Nucleation in liquids and solutions. *In*: Nucleation. Zettlemoyer AC (ed) Marcel Dekker, New York, p 225-307

Webb MA (1999) Cell-Mediated Crystallization of Calcium Oxalate in Plants. Plant Cell 11:751-761

Weiner S, Dove PM (2003) An overview of biomineralization processes and the problem of the vital effect. Rev Mineral Geochem 54:1-29

Wheeler AP, Low KC, Sikes CS (1990) $CaCO_3$ crystal-binding properties of peptides and their influence on crystal growth. *In:* Surface Reactive Peptides and Polymers: Discovery and Commercialization. Sikes CS, Wheeler AP (eds) ACS Books, Washington, ch. 6

Williams ED, Bartelt NC (1991) Thermodynamics of surface morphology. Science 251:393-400

Wilson DS, Dove PM, DeYoreo JJ (2002). Nanoscale effects of strontium on calcite growth: A baseline for understanding biomineralization in the absence of vital effects. Amer Geophys Union Fall Meeting Program, 228

Wong KK, Brisdon BJ, Heywood BR, Hodson GW, Mann S (1994) Polymer-mediated crystallisation of inorganic solids: Calcite nucleation on the surfaces of inorganic polymers. J Mater Chem 4:1387-1392

Yau S-T, Petsev DN, Thomas BR, Vekilov PG (2000a) Molecular-level thermodynamic and kinetic parameters for the self-assembly of apoferritin molecules into crystals. J Mol Biol 303: 667-678

Yau S-T, Thomas BR, Vekilov PG (2000b) Molecular mechanisms of crystallization and defect formation. Phys Rev Lett 85:353-356

Yau S-T, Vekilov PG (2000) Quasi-planar nucleus structure in apoferritin crystallisation. Nature 406:494-497

Yau S-T, Vekilov PG (2001) Direct observation of nucleus structure and nucleation pathways. J Am Chem Soc 123:1080-1089